

1 **NCBP2 modulates neurodevelopmental defects of the 3q29 deletion in**
2 ***Drosophila* and *X. laevis* models**

3

4 Short title: ***Drosophila* and *X. laevis* models of the 3q29 deletion**

5

6 Mayanglambam Dhruba Singh^{1*}, Matthew Jensen^{1*}, Micaela Lasser², Emily Huber¹, Tanzeen
7 Yusuff¹, Lucilla Pizzo¹, Brian Lifschutz¹, Inshya Desai¹, Alexis Kubina¹, Sneha Yennawar¹,
8 Sydney Kim², Janani Iyer¹, Diego E. Rincon-Limas³, Laura Anne Lowery², and Santhosh
9 Girirajan^{1,4}

10

- 11 1. Department of Biochemistry and Molecular Biology, Pennsylvania State University,
12 University Park, PA 16802 USA
- 13 2. Department of Biology, Boston College, Chestnut Hill, MA 02467 USA
- 14 3. Department of Neurology, McKnight Brain Institute, University of Florida,
15 Gainesville, FL 32611 USA
- 16 4. Department of Anthropology, Pennsylvania State University, University Park, PA
17 16802 USA

18

19 *contributed equally to the work

20

21 Correspondence:

22 Santhosh Girirajan, MBBS, PhD
23 205A Life Sciences Building
24 Pennsylvania State University
25 University Park, PA 16802
26 E-mail: sxg47@psu.edu
27 Phone: 814-865-0674

28

29

30 **ABSTRACT**

31 The 1.6 Mbp deletion on chromosome 3q29 is associated with a range of neurodevelopmental
32 disorders, including schizophrenia, autism, microcephaly, and intellectual disability. Despite
33 its importance towards neurodevelopment, the role of individual genes, genetic interactions,
34 and disrupted biological mechanisms underlying the deletion have not been thoroughly
35 characterized. Here, we used quantitative methods to assay *Drosophila melanogaster* and
36 *Xenopus laevis* models with tissue-specific individual and pairwise knockdown of 14
37 homologs of genes within the 3q29 region. We identified developmental, cellular, and
38 neuronal phenotypes for multiple homologs of 3q29 genes, potentially due to altered
39 apoptosis and cell cycle mechanisms during development. Using the fly eye, we screened for
40 314 pairwise knockdowns of homologs of 3q29 genes and identified 44 interactions between
41 pairs of homologs and 34 interactions with other neurodevelopmental genes. Interestingly,
42 *NCBP2* homologs in *Drosophila* (*Cbp20*) and *X. laevis* (*ncbp2*) enhanced the phenotypes of
43 homologs of the other 3q29 genes, leading to significant increases in apoptosis that disrupted
44 cellular organization and brain morphology. These cellular and neuronal defects were rescued
45 with overexpression of the apoptosis inhibitors *Diap1* and *xiap* in both models, suggesting
46 that apoptosis is one of several potential biological mechanisms disrupted by the deletion.
47 *NCBP2* was also highly connected to other 3q29 genes in a human brain-specific interaction
48 network, providing support for the relevance of our results towards the human deletion.
49 Overall, our study suggests that *NCBP2*-mediated genetic interactions within the 3q29 region
50 disrupt apoptosis and cell cycle mechanisms during development.

51

52 **AUTHOR SUMMARY**

53 Rare copy-number variants, or large deletions and duplications in the genome, are associated
54 with a wide range of neurodevelopmental disorders. The 3q29 deletion confers an increased
55 risk for schizophrenia, autism, and microcephaly. To understand the conserved biological
56 mechanisms that are disrupted by this deletion, we systematically tested 14 individual
57 homologs and 314 pairwise interactions of 3q29 genes for neuronal, cellular, and
58 developmental phenotypes in *Drosophila melanogaster* and *Xenopus laevis* models. We
59 found that multiple homologs of genes within the deletion region contribute towards
60 developmental defects, such as larval lethality and disrupted cellular organization.
61 Interestingly, we found that *NCBP2* acts as a key modifier gene within the region, enhancing
62 the developmental phenotypes of each of the homologs for other 3q29 genes and leading to
63 disruptions in apoptosis and cell cycle pathways. Our results suggest that multiple genes

64 within the 3q29 region interact with each other through shared mechanisms and jointly
65 contribute to neurodevelopmental defects.

66

67 **INTRODUCTION**

68 Rare copy number variants (CNVs), including deletions and duplications in the human
69 genome, significantly contribute to complex neurodevelopmental disorders such as
70 schizophrenia, intellectual disability/developmental delay, autism, and epilepsy [1,2]. Despite
71 extensive phenotypic heterogeneity associated with recently described CNVs [3], certain rare
72 CNVs have been linked to specific neuropsychiatric diagnoses. For example, the 22q11.2
73 deletion (DiGeorge/velocardiofacial syndrome), the most frequently occurring pathogenic
74 CNV, is found in about 1-2% of individuals with schizophrenia [4,5], and animal models of
75 several genes within the region show neuronal and behavioral phenotypes on their own [6,7].
76 Similarly, the 1.6 Mbp recurrent deletion on chromosome 3q29, encompassing 21 genes, was
77 initially identified in individuals with a range of neurodevelopmental features, including
78 intellectual disability, microcephaly, craniofacial features, and speech delay [8,9]. Further
79 studies have implicated this deletion as a major risk factor for multiple disorders [10]. In fact,
80 the deletion confers a >40-fold increase in risk for schizophrenia [11,12] as well as a >20-
81 fold increase in risk for autism [13]. More recently, two studies have reported decreases in
82 body and brain sizes as well as a range of behavioral and social defects in mouse models of
83 the entire deletion, mimicking the human developmental phenotypes associated with the
84 deletion [14,15].

85 Identifying the biological underpinnings of the 3q29 deletion is contingent upon
86 uncovering the conserved molecular mechanisms linking individual genes or combinations of
87 genes within the 3q29 region to the neurodevelopmental phenotypes observed in individuals
88 with the entire deletion. Recent studies have suggested a subset of genes in the 3q29 region as
89 potential candidates for these phenotypes based on their established roles in neuronal
90 development [16,17]. For example, *DLG1* is a scaffolding protein that organizes the synaptic
91 structure at neuromuscular junctions [18], affecting both synaptic density and plasticity
92 during development [19]. However, mouse models of *Dlg1*^{+/−} did not recapitulate the
93 behavioral and developmental phenotypes observed in mice with the entire deletion [14],
94 suggesting that haploinsufficiency of *DLG1* by itself does not account for the wide range of
95 phenotypes associated with the deletion. Given that genes within rare pathogenic CNV
96 regions tend to share similar biological functions [20] and interact with each other to
97 contribute towards developmental phenotypes [21,22], it is likely that multiple genes within
98 3q29 jointly contribute to these phenotypes through shared cellular pathways. Therefore, an
99 approach that integrates functional analysis of individual genes within the 3q29 deletion and

100 their combinatorial effects on neuronal and cellular phenotypes is necessary to understand the
101 pathways and mechanisms underlying the deletion.

102 Systematic testing of genes within 3q29 towards developmental and cellular
103 phenotypes requires model systems that are amenable for rapid phenotypic evaluation and
104 allow for testing interactions between multiple dosage-imbalanced genes without affecting
105 the viability of the organism. *Drosophila melanogaster* and *Xenopus laevis* provide such
106 powerful genetic models for studying conserved mechanisms that are altered in
107 neurodevelopmental disorders, with the ability to manipulate gene expression in a tissue-
108 specific manner in *Drosophila* [23] and examine developmental defects in *X. laevis* [24].
109 Both model systems contain homologs for a majority of disease-causing genes in humans,
110 and show a high degree of conservation in key developmental pathways [23,25–27]. For
111 example, *Drosophila* knockdown models of the candidate schizophrenia gene *DTNBPI*
112 showed dysregulation of synaptic homeostasis and altered glutamatergic and dopaminergic
113 neuron function [28,29], and fly models for *UBE3A*, the gene associated with Angelman
114 syndrome, showed sleep, memory and locomotor defects [30]. Furthermore, *X. laevis* models
115 have been widely used to identify morphological and neuronal defects associated with
116 developmental disorders [24], such as dendritic connectivity defects with overexpression of
117 *MECP2*, the causative gene for Rett syndrome [31]. Thus, *Drosophila* and *X. laevis* models
118 of individual CNV homologs and their interactions would allow for a deeper dissection of the
119 molecular mechanisms disrupted by the deletion, complementing the phenotypes documented
120 in mouse models of the entire deletion [14,15].

121 Here, we used a mechanistic approach to understand the role of individual homologs
122 of 3q29 genes and their interactions towards the cellular processes underlying the deletion.
123 We systematically characterized developmental, cellular, and nervous system phenotypes for
124 14 conserved homologs of human 3q29 genes and 314 pairwise interactions using
125 *Drosophila*, and validated these phenotypes using *X. laevis*. We found that multiple
126 homologs of genes within the 3q29 region, including *NCBP2*, *DLG1*, *FBXO45*, *PIGZ*, and
127 *BDH1*, contribute to disruptions in apoptosis and cell cycle pathways, leading to neuronal and
128 developmental defects in both model systems. These defects were further enhanced when
129 each of the homologs were concomitantly knocked down with homologs of *NCBP2* in
130 *Drosophila* (*Cbp20*) and *X. laevis* (*ncbp2*), resulting in increased apoptosis and dysregulation
131 of cell cycle genes. Our results support an oligogenic model for the 3q29 deletion, and
132 implicate specific cellular mechanisms disrupted by genes in the deletion region.

133 **RESULTS**

134 **Reduced expression of individual homologs of 3q29 genes causes global developmental**
135 **defects**

136 We used reciprocal BLAST and orthology prediction tools (see Methods) to identify fly
137 homologs for 15 of the 21 genes within the 3q29 deletion region (**Fig. 1, S1 Table**). We note
138 that the genes and crosses tested in this study are represented as fly gene names along with
139 the human counterparts at first mention in the text, i.e. *Cbp20* (*NCBP2*), and fly genes with
140 allele names in the figures, i.e. *Cbp20*^{KK109448}. We found that the biological functions of these
141 15 genes were also conserved between *Drosophila* and humans, as 61 of the 69 Gene
142 Ontology terms (88.4%) annotations for the human genes were also annotated for their
143 respective fly homologs (**S1 File**). For example, *dlg1* (*DLG1*) and *Cbp20* (*NCBP2*) share the
144 same roles in both flies and vertebrates, as a scaffolding protein at the synaptic junction [32]
145 and a member of the RNA cap binding complex [33], respectively. We used RNA
146 interference (RNAi) and the *UAS-GAL4* system to knockdown expression levels of fly
147 homologs of genes within the 3q29 region ubiquitously and in neuronal, wing and eye tissues
148 [**Fig. 1**]. A stock list of the fly lines used in this study and full genotypes for all
149 experiments are provided in **S2 File**. Quantitative PCR (qPCR) confirmed partial knockdown
150 of gene expression for each of the tested homologs (**S2 Table**); fly lines for *CG5359*
151 (*TCTEX1D2*) were excluded from further analysis after additional quality control assessment
152 (see Methods). To identify genes essential for organism survival and neurodevelopment, we
153 first assessed the effect of ubiquitous knockdown of homologs of 3q29 genes using the *da-*
154 *GAL4* driver (**Fig. 2A**). Seven of the 14 homologs, including *dlg1*, *Cbp20*, and *Tsf2* (*MFI2*),
155 showed lethality or severe developmental defects with ubiquitous knockdown, suggesting
156 that multiple homologs of 3q29 genes are essential for viability during early development.
157 Similarly, wing-specific *bx*^{MS1096}-*GAL4* knockdown of *Tsf2*, *Cbp20*, *CG8888* (*BDH1*), and
158 *Pak* (*PAK2*) showed severe wing defects, and wing-specific knockdown of *dlg1* showed
159 larval lethality (**S1 Fig.**).

160 Several fly homologs for genes within the 3q29 region have previously been
161 associated with a range of neuronal defects during fly development (**S3 Table**). For example,
162 loss of *dlg1* contributed to morphological and physiological defects at the neuromuscular
163 junction (NMJ), as well as increased brain size, abnormal courtship behavior, and loss of
164 gravitaxis response [35–37]. Similarly, *Pak* mutant flies exhibited extensive defects in the
165 axonal targeting of sensory and motor neurons [38,39], in addition to abnormal NMJ and
166 mushroom body development [40,41]. We sought to determine whether fly homologs for

167 other genes in the 3q29 region also contribute to defects in neuronal function, and therefore
168 performed climbing assays for motor defects and staining of larval brains for axonal targeting
169 with pan-neuronal knockdown of the fly homologs. Interestingly, *Elav-GAL4* mediated pan-
170 neuronal knockdown caused larval or pupal lethality in *dlg1*, *Tsf2*, and *CG5543 (WDR53)*
171 flies (**Fig. 2A**), and about 30% of adult flies with knockdown of *dlg1* did not survive beyond
172 day 5 (**S1 Fig.**), indicating an essential role for these genes in neuronal development.
173 Furthermore, we found that flies with pan-neuronal knockdown of several homologs of 3q29
174 genes, including *dlg1* and *Cbp20*, exhibited a strong reduction in climbing ability over ten
175 days (**Fig. 2B, S1 Video**), suggesting that these genes could contribute to abnormalities in
176 synaptic and motor functions [42]. We next examined the axonal projections of photoreceptor
177 cells into the optic lobe by staining third instar larval brains with anti-chaoptin. We found that
178 *GMR-GAL4* mediated eye-specific knockdown of *Cbp20*, *dlg1*, *Pak* and *Fsn (FBXO45)*
179 showed several axonal targeting defects (**S1 Fig., S4 Table**). Our results recapitulated the
180 previous findings in *Pak* mutant flies [38], and were similar to targeting defects observed in
181 models of other candidate neurodevelopmental genes, including *Drosophila* homologs for
182 human *DISC1* and *FMRI* [43,44]. Overall, our data show that multiple conserved homologs
183 of genes in the 3q29 region beyond just *dlg1* or *Pak* are important for *Drosophila*
184 neurodevelopment.

185

186 ***Drosophila* eye models for genes within the 3q29 region show cellular defects**

187 The *Drosophila* compound eye has been classically used to perform high-throughput genetic
188 screens and quantitative assays of cellular and neurodevelopmental defects [45]. In fact,
189 about two-thirds of all vital genes in the fly genome are predicted to be involved in fly eye
190 development [46]. For instance, the *Drosophila* eye model was recently used to screen a large
191 set of intellectual disability genes [47], and genetic interaction studies using the fly eye have
192 identified modifier genes for Rett syndrome, spinocerebellar ataxia type 3, and other
193 conserved developmental processes [48–50]. We used the developing fly eye as an *in vivo*
194 system to quantify the effect of gene knockdown on adult eye morphology, cellular
195 organization in the pupal eye, and cell proliferation and death in the larval imaginal eye disc
196 (**Fig. 1, S2 Fig.**). The wild-type adult *Drosophila* eye consists of about 750 ommatidia
197 containing different cell types arranged in a regular hexagonal structure, which can be easily
198 perturbed by genetic modifications [51,52]. Because of this, we first performed eye-specific
199 RNAi knockdown of fly homologs of genes in the 3q29 region using *GMR-GAL4*, and
200 measured the rough eye phenotype of each knockdown line using *Flynotyper*, a quantitative

201 tool that calculates a phenotypic score based on defects in ommatidial arrangement [53]. We
202 found that eye-specific knockdown of 8/13 homologs of 3q29 genes showed significant
203 external eye phenotypes compared with control *GMR-GAL4* flies, while knockdown of *Tsf2*
204 caused lethality (**Fig. 2C, S3 Fig.**). For example, knockdown of *Cbp20* resulted in a severe
205 rough eye phenotype that was comparable to knockdown of other neurodevelopmental genes
206 [53], such as *Prosap* (*SHANK3*) and *kis* (*CHD8*) (**S5 Table**).

207 To examine the cellular mechanisms underlying the rough eye phenotypes observed
208 with knockdown of fly homologs of 3q29 genes, we first measured changes in area and
209 ommatidial size of the adult eyes. We found a significant reduction in eye size with
210 knockdown of *CG8888* and *Cbp20*, while the eyes of flies with knockdown of *dlg1* were
211 significantly larger than *GMR-GAL4* controls (**Fig. 2D**). Similarly, we observed decreases in
212 ommatidial diameter with knockdown of *Cbp20* and *CG8888*, suggesting that these genes
213 may also contribute to abnormal cell growth phenotypes (**S3 Fig.**). We also assessed the
214 cellular structure of 44 hour-old pupal eyes by staining the ommatidial and photoreceptor
215 cells with anti-DLG, a septate junction marker, and Phalloidin, a marker for F-actin at cell
216 boundaries (**S2 Fig.**). We found that knockdown of 11/12 tested homologs of 3q29 genes
217 caused disorganization or loss of the photoreceptor neurons and ommatidial cells (**Fig. 2E, S4**
218 **Fig., S6 Table**). For example, pupal eyes with knockdown of *CG8888*, *dlg1*, *Cbp20* and
219 *CG5543* all showed defects in cone cell orientation and ommatidial rotation compared with
220 control *GMR-GAL4* flies. Furthermore, *Cbp20* and *dlg1* knockdown flies showed hexagonal
221 defects and severe disorganization of photoreceptor neurons, while *Cbp20* knockdown flies
222 also showed fused secondary cells and *dlg1* knockdown flies showed a complete loss of
223 bristle cells.

224 We next hypothesized that abnormal proliferation and apoptosis could contribute to
225 the cellular defects observed with knockdown of fly homologs of 3q29 genes. To test this, we
226 stained the third instar larval eye discs for select knockdowns of individual homologs of 3q29
227 genes with anti-pH3 (phospho-Histone H3 (Ser10)) and *Drosophila* caspase-1 (dcp1),
228 markers for proliferating and apoptotic cells, and quantified the number of cells posterior to
229 the morphogenetic furrow (**S2 Fig.**). We observed a significant decrease in pH3-positive cells
230 for *CG8888* knockdown flies and trends towards increased pH3-positive cells for *PIG-Z*
231 (*PIGZ*) knockdown flies compared with *GMR-GAL4* controls ($p=0.165$) (**Fig. 2F, S4 Fig.**),
232 while knockdown of *dlg1* led to significant increases in cells stained with bromodeoxyuridine
233 (BrdU), a marker for replicating cells (**S4 Fig.**). Flies with knockdown of *Cbp20* or *dlg1* also
234 showed a significant increase in apoptotic dcp1-positive cells compared with controls (**Fig.**

235 **2G**), which we validated using TUNEL assays for these lines (**S4 Fig.**). We further tested for
236 proliferation and apoptosis in the third instar larval wing discs of flies with knockdown of
237 homologs of 3q29 genes using the *bx^{MS1096}-GAL4* driver, and observed changes in both
238 processes with knockdown of *dlg1*, *CG8888* and *Cbp20* (**S5 Fig.**). Knockdown of *Cbp20* in
239 particular showed dcp1-positive staining across the entire wing pouch in the larval wing disc.
240 These data suggest that knockdown of multiple fly homologs of genes in the 3q29 region
241 contribute to defects in apoptosis and proliferation during early development, leading to the
242 observed defects in cell count and organization (**Table 1**).

243

244 **Interactions between fly homologs of 3q29 genes enhance neuronal phenotypes**

245 As knockdown fly models for homologs of multiple 3q29 genes showed a variety of
246 neuronal, developmental, and cellular defects, we hypothesized that these genes could
247 interact with each other to further disrupt cellular processes during development. We
248 therefore generated *GMR-GAL4* recombined lines for nine fly homologs of 3q29 genes, and
249 crossed these lines with multiple RNAi or mutant lines for other homologs to generate 161
250 two-hit crosses for testing 94 pairwise gene interactions (**Fig. 1, S7 Table**). We found a
251 significant enhancement in eye phenotypic severity, measured using *Flynotyper* and validated
252 with a second line when available, for 39 pairwise knockdowns compared with recombined
253 lines crossed with control flies (represented in the figures as *Cbp20^{KK109448}/Control*) (**Fig. 3A**,
254 **S6 Fig.**, **S7 Fig.**). In fact, we found that 19 out of 21 pairwise interactions involving *Cbp20* as
255 either a first or second-hit gene resulted in more severe eye phenotypes, suggesting that
256 reduced expression of *Cbp20* drastically modifies the morphological phenotypes of other
257 homologs of 3q29 genes (**Fig. 3B-D**). For further validation, we compared pairs of reciprocal
258 crosses (i.e. *Fsn/CG8888* versus *CG8888/Fsn*) and confirmed concordant results for 19/26
259 reciprocal interactions, including 14/16 reciprocal interactions involving *Cbp20* (**S7 Table**).
260 We also found a non-significant increase in severity for *dlg1/Pak* knockdown flies using both
261 RNAi and mutant lines, concordant with enhanced neuromuscular junction and circadian
262 rhythm defects observed in mutant *dlg1/Pak* flies described by Grice and colleagues [54].

263 As *Cbp20* knockdown enhanced the rough eye phenotypes of multiple other
264 homologs, we next tested for enhancement of neuronal defects among flies with knockdown
265 of *Cbp20* and homologs of other 3q29 genes. We found that simultaneous knockdown of
266 *Cbp20* with *dlg1* or *Fsn* led to an increase in severity of axon targeting defects (**Fig. 3E**). For
267 instance, while knockdown of *Cbp20* mostly led to mild-to-moderate axon targeting defects,
268 such as loss of R7-R8 axon projection into the medulla, we observed more severe loss of

269 projection for all axons with simultaneous knockdown of *Cbp20* and *dlg1* or *Fsn* (**S4 Table**).
270 We also tested pan-neuronal *Elav-GAL4* knockdown of select pairs of homologs, and found
271 that both *Cbp20/dlg1* and *Cbp20/Fsn* significantly enhanced the climbing defects observed
272 with knockdown of *Cbp20* alone (**Fig. 3F, S2 Video**). Overall, these data show that *Cbp20*
273 interacts with other homologs of genes in the 3q29 region to enhance the observed cellular
274 and neuronal defects (**Table 1**).

275 To further characterize the functional effects of interactions between homologs of
276 3q29 genes, we analyzed changes in gene expression by performing RNA-sequencing of
277 heads from flies with select pan-neuronal knockdown of individual (*Cbp20*, *dlg1*, *Fsn*, and
278 *Pak*) and pairs (*Cbp20/dlg1* and *Cbp20/Fsn*) of homologs of 3q29 genes. We identified
279 differentially-expressed genes in each of the tested fly models compared with *Elav-GAL4*
280 controls, and performed enrichment analysis on both differentially-expressed fly genes and
281 their corresponding human homologs (**S3 File**). We found that knockdown of each individual
282 homolog showed enrichment for dysregulation of cellular and developmental processes (**S8**
283 **Fig.**). For example, flies with knockdown of *dlg1* and *Cbp20* showed enrichment for
284 dysregulation of homologs for human synaptic transmission genes, such as *Glt* (*NLGN1*) and
285 *nAChRβ3* (*HTR3A*). Furthermore, flies with knockdown of *Cbp20* were enriched for
286 dysregulated fly genes related to metabolic processes, while knockdown of *Fsn* led to
287 dysregulation of fly genes involved in response to external stimuli and immune response. We
288 also found that homologs of key signaling genes dysregulated in mouse models of the 3q29
289 deletion, reported by Baba and colleagues [15], were differentially expressed in our fly
290 models for homologs of 3q29 genes. In fact, knockdown of *Fsn* led to altered expression for
291 each of the “early immediate” signaling genes dysregulated in the deletion mouse model [15].
292 While dysregulated genes in *Cbp20/dlg1* knockdown flies showed enrichments for protein
293 folding and sensory perception, *Cbp20/Fsn* knockdown flies were uniquely enriched for
294 dysregulated homologs of cell cycle genes, including *Aura* (*AURKA*), *Cdk1* (*CDK1*), *lok*
295 (*CHEK2*), and *CycE* (*CCNE1*) (**S8 Fig.**). We similarly found 17 differentially-expressed
296 homologs corresponding to human apoptosis genes in *Cbp20/Fsn* knockdown flies, including
297 the DNA fragmentation gene *Sid* (*ENDOG*) and the apoptosis signaling genes *tor* (*RET*) and
298 *Hsp70Bb* (*HSPA1A*). Furthermore, we found a strong enrichment for fly genes whose human
299 homologs are preferentially expressed in early and mid-fetal brain tissues among the
300 dysregulated genes in *Cbp20/Fsn* knockdown flies (**S8 Fig.**). These data suggest that *Cbp20*
301 interacts with other homologs of genes in the 3q29 region to disrupt a variety of key

302 biological functions, including apoptosis and cell cycle pathways as well as synaptic
303 transmission and metabolic pathways (**Table 1**).

304 Finally, to complement the interactions among homologs of 3q29 genes that we
305 identified in *Drosophila*, we examined the connectivity patterns of 3q29 genes within the
306 context of human gene interaction databases. Gene interaction networks derived from co-
307 expression and protein-protein interaction data [55,56] showed large modules of connected
308 genes within the 3q29 region, including a strongly-connected component involving 11/21
309 3q29 genes (**Fig. 4A-B**). However, the average connectivity among 3q29 genes within a
310 brain-specific interaction network [57] was not significantly different from the connectivity
311 of randomly-selected sets of genes throughout the genome (**Fig. 4C**), suggesting that a subset
312 of genes drive the complexity of genetic interactions within the region. This paradigm was
313 previously observed among genes in the 22q11.2 deletion region, where interactions between
314 *PRODH* and *COMT* modulate neurotransmitter function independently of other genes in the
315 region [58]. In fact, five genes in the 3q29 region, including *NCBP2*, *PAK2*, and *DLG1*,
316 showed significantly higher connectivity to other 3q29 genes compared with the average
317 connectivity of random sets of genes (**Fig. 4D**). Interestingly, *NCBP2* showed the highest
318 connectivity of all genes in the region, further highlighting its role as a key modulator of
319 genes within the region.

320

321 **Interactions between *Cbp20* and other homologs of 3q29 genes enhance apoptosis 322 defects**

323 Cell death and proliferation are two antagonistic forces that maintain an appropriate number
324 of neurons during development [59]. In fact, both processes have been previously identified
325 as candidate mechanisms for several neurodevelopmental disorders [60–62]. While
326 knockdown of *Cbp20* with other homologs of 3q29 genes likely disrupts multiple cellular
327 processes that contribute towards the enhanced cellular defects, we next specifically
328 investigated the role of apoptosis towards these defects, as larval eye and wing discs with
329 knockdown of *Cbp20* showed strong increases in apoptosis. We observed black necrotic
330 patches on the ommatidia in adult eyes with knockdown of *Cbp20/dlg1* and *Cbp20/Fsn*,
331 indicating that an increase in cell death occurs with these interactions (**Fig. 5A, S9 Fig.**). In
332 fact, significantly larger regions of necrotic patches were observed in flies homozygous for
333 *Cbp20* RNAi and heterozygous for *dlg1* RNAi (see **S2 File** for full genotype annotation),
334 suggesting that the knockdown of both homologs contributes to ommatidial cell death (**Fig.**
335 **5A**). Furthermore, we found an enhanced disruption of ommatidial cell organization and loss

336 of photoreceptors in pupal flies with concomitant knockdown of *Cbp20* with *dlg1*, *Fsn* or
337 *CG8888*, emphasizing the role of these genes in maintaining cell count and organization (**Fig.**
338 **5B-C, S9 Fig., S8 Table**). Based on these observations, we next assayed for apoptotic cells in
339 the larval eye discs of flies with knockdown of *Cbp20* and other homologs of 3q29 genes. We
340 observed significant increases in the number of apoptotic cells, as measured by *dcp1* (**Fig.**
341 **5D-E**) and TUNEL staining (**S9 Fig.**), when *Cbp20* was knocked down along with *CG8888*,
342 *dlg1*, or *Fsn*. *Cbp20/CG8888* knockdown flies also showed a decreased number of pH3-
343 positive cells, suggesting that both apoptosis and proliferation are affected by the interaction
344 between these two genes (**Fig. 5F**).

345 To validate apoptosis as a candidate mechanism for the cellular defects of flies with
346 knockdown of homologs of 3q29 genes, we crossed recombined fly lines for *Cbp20* and *dlg1*
347 with flies overexpressing *Diap1* (death-associated inhibitor of apoptosis). *Diap1* is an E3
348 ubiquitin ligase that targets *Dronc*, the fly homolog of caspase-9, and prevents the subsequent
349 activation of downstream caspases that lead to apoptosis [63]. We found that overexpression
350 of *Diap1* rescued the adult rough eye phenotypes (**Fig. 6A-B, S10 Fig.**) and increased the eye
351 sizes of *Cbp20* and *dlg1* flies (**S10 Fig.**). These observations were corroborated by the
352 reversal of cellular changes in the eye upon *Diap1* overexpression, including the rescue of
353 ommatidial structure and cell count deficits observed with knockdown of *Cbp20* and *dlg1*
354 (**Fig. 6D, S10 Fig.**). Furthermore, overexpression of *Diap1* led to significant reductions in the
355 number of TUNEL and *dcp1*-positive cells in the larval eye discs of flies with knockdown of
356 *Cbp20* and *dlg1*, confirming the rescue of apoptosis defects in these flies (**Fig. 6E-F, S10**
357 **Fig.**). Interestingly, *Diap1* overexpression also suppressed the photoreceptor axon targeting
358 defects observed with knockdown of *Cbp20* (**Fig. 6G, S4 Table**), suggesting that the
359 neuronal defects observed in these flies could be attributed to increased apoptosis. We further
360 confirmed these mechanistic findings by observing increased severity in cellular phenotypes
361 upon overexpression of *Dronc* in *Cbp20* and *dlg1* knockdown flies. For example, we
362 observed black necrotic patches (**Figs. 6A and 6C**) and exaggerated apoptotic responses (**Fig.**
363 **6E-F, S10 Fig.**) in *Cbp20* knockdown flies with overexpression of *Dronc*. These results
364 suggest that apoptosis mediates the cellular defects observed in flies with knockdown of
365 *Cbp20* and *dlg1*.

366

367 **Homologs of 3q29 genes interact with canonical neurodevelopmental genes**

368 We further explored the role of 3q29 genes in neurodevelopmental pathways by screening
369 four fly homologs with strong neurodevelopmental phenotypes (*Cbp20*, *dlg1*, *CG8888*, and

370 *Pak*) for interactions with homologs of 15 known human neurodevelopmental genes, for a
371 total of 60 pairwise interactions and 153 two-hit crosses (**Fig. 7A**). We selected these
372 neurodevelopmental genes for screening based on their association with developmental
373 disorders in humans [53,64], and included eight genes associated with apoptosis or cell cycle
374 functions as well as four genes associated with microcephaly [65], a key phenotype observed
375 in approximately 50% of 3q29 deletion carriers [8]. We found that 34 pairwise interactions,
376 validated with a second line when available, led to significant increases in eye phenotypes
377 compared with recombined lines for individual homologs of 3q29 genes (**S9 Table, S11**
378 **Fig.**). These interactions included 19 validated interactions of homologs of 3q29 genes with
379 apoptosis or cell cycle genes as well as ten interactions with microcephaly genes. We found
380 that 13/15 homologs of neurodevelopmental genes, including all four microcephaly genes,
381 enhanced the phenotypes observed with knockdown of *Cbp20* alone. Furthermore,
382 knockdown of *dlg1* significantly enhanced the ommatidial necrotic patches observed with
383 knockdown of *arm* (*CTNNB1*), while flies with concomitant knockdown of *Cbp20* and *arm*
384 also showed increased necrotic patches (**Fig. 7B, S9 Fig.**). Interestingly, we also found that
385 knockdown of *CG8888* and *dlg1* suppressed the rough eye phenotypes observed with
386 knockdown of *Prosap* (*SHANK3*), while knockdown of *Pak* suppressed the phenotypes of
387 both *Prosap* and *Pten* (*PTEN*) knockdown flies (**Fig. 7B**). Several of these interactions have
388 been previously observed to modulate neuronal function in model systems. For example,
389 *SHANK3* interacts with *DLG1* through the mediator protein DLGAP1 to influence post-
390 synaptic density in mice [66] and binds to proteins in the Rac1 complex, including PAK2, to
391 regulate synaptic structure [67,68]. These results suggest that homologs of 3q29 genes
392 interact with key developmental genes in conserved pathways to modify cellular phenotypes.
393

394 **Reduction of 3q29 gene expression causes developmental defects in *Xenopus laevis***
395 After identifying a wide range of neurodevelopmental defects due to knockdown of fly
396 homologs of 3q29 genes, we sought to gain further insight into the conserved functions of
397 these genes in vertebrate embryonic brain development using the *Xenopus laevis* model
398 system. We examined the effect of targeted knockdown of *ncbp2*, *fbxo45*, and *pak2*, as
399 homologs of these genes displayed multiple severe phenotypes with reduced gene expression
400 in flies. Knockdown of *X. laevis* homologs for each 3q29 gene was accomplished using
401 antisense morpholino oligonucleotides (MOs) targeted to early splice sites of each homolog
402 (**Fig. 1**). *X. laevis* embryos were injected at either the two- or four-cell stage with various
403 concentrations of MO for each homolog or a standard control, and knockdown of each

404 homolog was validated using qPCR (**S12 Fig.**). As knockdown of *Cbp20*, *Fsn*, and *Pak* each
405 resulted in neuronal defects in *Drosophila*, we first examined the effects of knockdown of
406 these homologs on *X. laevis* brain development at stage 47. To test this, we knocked down
407 each gene in half of the embryo at the two-cell stage, and left the other half uninjected to
408 create a side-by-side comparison of brain morphology (**Fig. 8A**). We performed whole-mount
409 immunostaining with anti-alpha tubulin and found that reduced expression of *ncbp2*, *fbxo45*,
410 and *pak2* each resulted in smaller forebrain and midbrain size compared with controls (**Fig.**
411 **8A-C**). We also found that simultaneous knockdown of *ncbp2* with *fbxo45* caused a
412 significant decrease in forebrain size and a trend towards decreased midbrain size ($p=0.093$)
413 compared with *ncbp2* knockdown (**Fig. 8A-C**). Knockdown of *pak2* with *ncbp2* showed a
414 similar trend towards decreased forebrain size ($p=0.051$). Interestingly, the reduced brain
415 volumes we observed with knockdown of homologs of 3q29 genes in *X. laevis* recapitulate
416 the reduced brain volume observed in 3q29 deletion mice [14,15], suggesting that multiple
417 genes in the 3q29 region contribute to this phenotype. We further examined the effect of
418 knocking down homologs of 3q29 genes on *X. laevis* eye development at stage 42, and found
419 that knockdown of these homologs caused irregular shapes and decreased size compared with
420 controls (**S13 Fig.**). The reductions in eye size were rescued to control levels when mRNA
421 was co-injected along with MO for each homolog (**S13 Fig.**). Together, these data show that
422 individual and pairwise knockdown of homologs of 3q29 genes in *X. laevis* leads to abnormal
423 brain and eye morphology, confirming the conserved role of these genes during vertebrate
424 development.

425 To determine if the knockdown of homologs of 3q29 genes also disrupted apoptotic
426 processes in *X. laevis*, we tested whether overexpression of the X-linked inhibitor of
427 apoptosis gene (*xiap*) could rescue the observed developmental defects. We found that
428 overexpression of *xiap* rescued the midbrain and forebrain size deficits observed with *ncbp2*
429 knockdown to control levels (**Fig. 8A-C**). Similarly, we found that the decreased eye sizes
430 and morphological defects observed with knockdown of *ncbp2* were rescued with *xiap*
431 overexpression (**S13 Fig.**). To further validate these findings, we performed a western blot
432 following knockdown of *fbxo45* and *ncbp2* using anti-cleaved caspase-3 (Asp175) as a
433 marker for apoptosis (**Fig. 8D, S12 Fig.**). We found that reduction of *fbxo45* and *ncbp2*
434 expression each led to an increase in cleaved caspase-3 levels compared with controls, which
435 were restored to control levels with concomitant overexpression of *xiap* (**Fig. 8E**). Caspase-3
436 levels were also enhanced when *fbxo45* and *ncbp2* were knocked down together (**Fig. 8E**),
437 suggesting that these two homologs interact with each other and contribute towards

438 developmental phenotypes through increased apoptosis. Overall, these results suggest
439 involvement of apoptotic processes towards the developmental phenotypes observed with
440 knockdown of homologs of 3q29 genes in a vertebrate model (**Table 1**).
441

442 **DISCUSSION**

443 Using complementary *Drosophila* and *X. laevis* models, we interrogated developmental
444 effects, cellular mechanisms, and genetic interactions of individual homologs of genes within
445 the 3q29 region. Our major findings were recapitulated across both model systems (**Table 1**)
446 and could also potentially account for the developmental phenotypes reported in mouse
447 models of the entire deletion. Several themes have emerged from our study that exemplify the
448 genetic and mechanistic complexity of the 3q29 deletion region.

449 *First*, our analysis of developmental phenotypes with knockdown of homologs for
450 individual 3q29 genes showed that a single gene within the region may not be solely
451 responsible for the effects of the deletion. In fact, we found that knockdown of 12 out of 14
452 fly homologs showed developmental defects in *Drosophila*, while every fly homolog showed
453 an enhanced rough eye phenotype when knocked down along with at least one other homolog
454 (**Fig. 2**). Although our study is limited to examining conserved cellular phenotypes of
455 homologs of 3q29 genes in *Drosophila* and *X. laevis*, evidence from other model organisms
456 also supports an oligogenic model for the deletion. In fact, knockout mouse models for
457 several 3q29 genes have been reported to exhibit severe developmental phenotypes, including
458 axonal and synaptic defects in *Fbxo45*^{-/-} and embryonic lethality in *Pak2*^{-/-} and *Pcyt1a*^{-/-}
459 knockout mice [69–71] (**S3 Table**). Notably, although *Dlg1*^{+/+} or *Pak2*^{+/+} mice showed a
460 range of neuronal phenotypes compared with control mice, they did not recapitulate the major
461 developmental and behavioral features observed in mouse models of the entire deletion
462 [14,15,72], suggesting that the deletion phenotypes are contingent upon haploinsufficiency of
463 multiple genes in the region (**S10 Table**). Furthermore, several 3q29 genes including *PAK2*,
464 *DLG1*, *PCYT1A*, and *UBXN7* are under evolutionary constraint in humans, based on gene
465 pathogenicity metrics (**S1 File**). Two genes in the 3q29 region without fly homologs, *CEP19*
466 and *TFRC*, are also under evolutionary constraint in humans, with *TFRC* having been
467 implicated in neural tube defects and embryonic lethality in mouse models [73]. While no
468 common variants associated with neurodevelopmental traits have been observed in the 3q29
469 region [74], rare variants of varying effects in 9/21 genes have been identified among patients
470 with different developmental disorders [75–77] (**S1 File**). These data, combined with our
471 findings in *Drosophila* and *X. laevis*, implicate multiple genes within the 3q29 region as
472 potential candidates for neurodevelopmental defects.

473 *Second*, our screening of 161 crosses between pairs of fly homologs of 3q29 genes
474 identified 44 interactions that showed enhanced rough eye phenotypes, suggesting that
475 complex interactions among genes in the 3q29 region could contribute towards

476 developmental defects (**Fig. 9A**). While we only tested a subset of all possible interactions
477 among the non-syntenic homologs of 3q29 genes in *Drosophila*, our results highlight
478 conserved mechanistic relationships between “parts”, or the individual genes, towards
479 understanding the effects of the “whole” deletion. For example, knockdown of *Cbp20*
480 enhanced the phenotypes of 11 out of 12 other fly homologs, suggesting that *NCBP2* could be
481 a key modulator of other genes within the region. *NCBP2* encodes a subunit of the nuclear
482 cap-binding complex (CBC), which binds to the 5' end of mRNA and microRNA in the
483 nucleus [78]. Given the role of the CBC in post-transcriptional regulatory mechanisms such
484 as nonsense-mediated decay, alternative splicing and mRNA transport [79,80], it is possible
485 that disruption of this complex could result in changes to a broad set of genes and biological
486 processes. In fact, our analysis of differentially-expressed genes in *Cbp20* knockdown flies
487 showed disruption of synaptic transmission, cellular respiration, and several metabolic
488 pathways. In contrast to other proposed candidate genes in the 3q29 region, *NCBP2* is not
489 predicted to be pathogenic on its own in humans (**S1 File**) and does not have identified
490 deleterious mutations in sequencing studies of neurodevelopmental disease cohorts so far,
491 indicating its potential role as a modifier of the other candidate genes in the region (**Fig. 9B**).
492 Our results also complement previous reports of synergistic interactions among fly homologs
493 of 3q29 genes in the nervous system [54], representing another hallmark of an oligogenic
494 model for the deletion. As these genetic interactions may vary across different species,
495 developmental timepoints, and tissues, the role of these interactions should be more deeply
496 explored using mouse and human cell culture models.

497 *Third*, we identified disruptions to several cellular processes due to both single and
498 pairwise knockdown of homologs in *Drosophila* and *X. laevis* models (**Table 1**). For
499 example, simultaneous knockdown of homologs of *NCBP2* and *FBXO45* in *Drosophila* led to
500 enhanced cellular disorganization (**Fig. 5**) and altered expression of cell cycle and apoptosis
501 genes (**S8 Figure**), as well as enhanced morphological defects and increased caspase-3 levels
502 in *X. laevis* (**Fig. 8**). We further found that overexpression of the apoptosis inhibitors *Diap1*
503 and *xiap* rescued the cellular and neuronal phenotypes observed with knockdown of
504 homologs of 3q29 genes (**Fig. 6**), providing important validations for the potential
505 involvement of apoptosis in the deletion (**Table 1**). We propose that *NCBP2* could modify
506 several cellular and molecular processes that may not be directly related to apoptosis, but
507 could instead lead to a cascade of biological events that ultimately result in apoptosis (**Fig.**
508 **9B**). Apoptosis mechanisms are well-conserved between *Drosophila*, *X. laevis*, and humans,
509 with key genes such as *XIAP* (*Diap1*), *CASP2* (*Dronec*), *CASP3* (*DrICE*), and *CASP7* (*Dcp-1*)

sharing the same roles in programmed cell death across the three organisms [81–83]. In fact, we found that fly homologs of human genes annotated for apoptosis function in the Gene Ontology database were also enriched for apoptosis function (n=1,063 fly homologs from 1,789 human apoptosis genes; $p=5.30\times10^{-13}$, Fisher's Exact test with Benjamini-Hochberg correction). Although we focused on testing apoptosis phenotypes with knockdown of homologs of 3q29 genes, we note that apoptosis is potentially one of many cellular pathways disrupted by the 3q29 deletion (**Fig. 9B**). In fact, our data implicated knockdown of several homologs of 3q29 genes, including *dlg1* and *CG8888 (BDHI)*, towards abnormal cell proliferation during development. Furthermore, several 3q29 genes have been previously associated with apoptosis or cell cycle regulation functions (**S1 File**). For example, *DLG1* is a tumor suppressor gene whose knockdown in *Drosophila* leads to neoplasms in the developing brain and eye disc [84,85], while *PAK2* is a key downstream mediator of the ERK signaling pathway for neuronal extension and is activated by caspases during apoptosis [70,86,87]. Our results recapitulate the role of *DLG1* towards cell cycle regulation, and also implicate *NCBP2* and its interactions towards multiple cellular and developmental phenotypes.

More broadly, genes involved with apoptosis and cell proliferation have been implicated in several neurodevelopmental disorders. For example, we previously observed disrupted cell proliferation upon knockdown of *Drosophila* homologs of genes in the 16p11.2 deletion region, as well as an enrichment of cell cycle function among connector genes between pairs of 16p11.2 genes in a human brain-specific network [21]. Furthermore, abnormal apoptosis in the early developing brain has been suggested as a possible mechanism for the decreased number of neurons observed in individuals with autism and schizophrenia [62,88,89]. For example, increased apoptosis was observed in both postmortem brain tissue from autism patients [90] and primary fibroblasts from schizophrenia patients [91,92]. We found further support for the role of apoptosis in these disorders by identifying significant enrichments for genes associated with apoptotic processes among candidate genes for autism (empirical $p<1.00\times10^{-5}$) [77], intellectual disability ($p<1.00\times10^{-5}$) [93], and schizophrenia ($p=0.014$) [76] (**S11 Table**). In fact, out of the 525 neurodevelopmental genes involved in apoptosis, 20 genes were present within pathogenic CNV regions [94], including *CORO1A*, *MAPK3* and *TAOK2* in the 16p11.2 region as well as *TBX1*, the causative gene for heart defects in DiGeorge/velocardiofacial syndrome [95] (**S4 File**). In addition to neuropsychiatric disorders, apoptosis has also been implicated in syndromic forms of microcephaly in humans [96] as well as decreased brain size in animal models of microcephaly genes [97,98]. For example, a mouse model of the Nijmegen breakage syndrome gene *NBN* exhibited increased

544 neuronal apoptosis, leading to microcephaly and decreased body mass [99]. Overall, these
545 findings highlight the importance of cell cycle-related processes, particularly apoptosis and
546 proliferation, towards modulating neuronal phenotypes that could be responsible for
547 developmental disorders.

548 In this study, the use of *Drosophila* and *X. laevis* models, both of which are amenable
549 to high-throughput screening of developmental phenotypes, allowed us to systematically
550 examine the conserved cellular and mechanistic roles of homologs of 3q29 genes and their
551 interactions. Follow-up studies in more evolutionarily advanced systems, such as mouse or
552 human cell lines, will be useful to overcome limitations of *Drosophila* and *X. laevis* models,
553 including testing the neurodevelopmental phenotypes and interactions of 3q29 genes without
554 fly homologs. Collectively, these results emphasize the utility of quantitative functional
555 assays for identifying conserved pathways associated with neurodevelopmental disorders,
556 which will hopefully allow for future discoveries of treatments for these disorders.

557

558 **MATERIALS AND METHODS**

559 **Fly stocks and genetics**

560 Using reciprocal BLAST searches and orthology predictions from the *DIOPT* v.7.1 database
561 [100], we identified 15 fly homologs for the 21 human genes within the chromosome 3q29
562 region (**S1 Table**). No fly homologs were present for six genes, including *LRRC33*, *CEP19*,
563 *RNF168*, *SMCO1*, *TFRC*, and *TM4SF19*. We used a similar strategy to identify homologs for
564 other neurodevelopmental genes tested for interactions in this study. Gene Ontology-Slim
565 (GO-Slim) terms for each human gene and fly homolog were obtained from PantherDB [101]
566 and are provided in **S1 File**. RNAi lines for fly homologs were obtained from the Vienna
567 Drosophila Resource Centre [102] (VDRC), including both KK and GD lines, and the
568 Bloomington *Drosophila* Stock Center (BDSC) (NIH P40OD018537). A list of fly RNAi
569 lines used in this study is provided in **S2 File**. Fly RNAi lines for homologs of 3q29 genes
570 were tested for gene knockdown using quantitative PCR (**S1 Table**). As the available KK line
571 for CG5359 (*TCTEX1D2*) showed a wing phenotype consistent with *tiptop* overexpression
572 due to RNAi insertion at the 5'UTR of the gene [103], which we confirmed using qPCR
573 analysis (**S5 File**), we excluded this gene from our experiments. Microarray data and
574 modENCODE Anatomy RNA-Seq from FlyBase [104,105] showed that all of the 14 tested
575 homologs were expressed in the fly central nervous system and eye tissues (**S1 Table**).

576 All fly stocks and crosses were cultured on conventional cornmeal-sucrose-dextrose-
577 yeast medium at 25°C, unless otherwise indicated. RNAi lines were crossed with a series of
578 *GAL4* driver lines to achieve tissue-specific knockdown of genes, including *w¹¹¹⁸;da-GAL4*
579 (Scott Selleck, Penn State) for ubiquitous, *w¹¹¹⁸;dCad-GFP*, *GMR-GAL4/CyO* (Zhi-Chun Lai,
580 Penn State) and *w¹¹¹⁸;GMR-GAL4;UAS-Dicer2* (Claire Thomas, Penn State) for eye-specific,
581 *w¹¹¹⁸;bx^{MS1096}-GAL4;UAS-Dicer2* (Zhi-Chun Lai, Penn State) for wing-specific, and
582 *w¹¹¹⁸;Elav-GAL4* (Mike Groteweil, VCU) and *w¹¹¹⁸;Elav-GAL4;UAS-Dicer2* (Scott Selleck,
583 Penn State) for pan-neuronal knockdown of gene expression. A list of full genotypes for all
584 crosses tested in this study is provided in **S2 File**. To perform interaction studies, we
585 generated recombined stock lines of *GMR-GAL4* with reduced expression of nine select
586 homologs of 3q29 genes (**S2 File**). Females from these stocks with constitutively reduced
587 gene expression for each of these genes were crossed with RNAi lines of other homologs to
588 achieve simultaneous knockdown of two genes (**Fig. 1**). We previously demonstrated that
589 these two-hit crosses had adequate *GAL4* to bind to two independent *UAS-RNAi* constructs
590 [21].

591

592 **Quantitative polymerase chain reaction for *Drosophila* RNAi knockdowns**

593 Levels of gene expression knockdown were confirmed using quantitative reverse-
594 transcriptase PCR (qPCR) on RNA isolated from pooled groups of 35 fly heads per line
595 tested (**S2 Table**). Briefly, RNAi lines were crossed with *Elav-GAL4* (to test RNAi line
596 efficacy) or *Elav-GAL4;;UAS-Dicer2* (to test for *tiptop* overexpression) at 25°C to achieve
597 pan-neuronal knockdown of the fly homolog. Adult fly heads at day 3 were separated by
598 vortexing, and total RNA was isolated using TRIzol (Invitrogen, Carlsbad, CA, USA). cDNA
599 was prepared using the qScript cDNA synthesis kit (Quantabio, Beverly, MA, USA).
600 Quantitative PCR was performed using an Applied Biosystems Fast 7500 system with SYBR
601 Green PCR master mix (Quantabio) to estimate the level of gene expression. All experiments
602 were performed using three biological replicates of 35 fly heads each. Primers were designed
603 using NCBI Primer-BLAST [106], with primer pairs separated by an intron in the
604 corresponding genomic DNA. A list of primers used in the experiments is provided in **S2**
605 **Table**. The delta-delta Ct value method was used to obtain the relative expression of fly
606 homologs in the RNAi lines compared with *Elav-GAL4* controls [107].

607

608 **Climbing assay**

609 We set up fly crosses at 25°C with *Elav-GAL4* to obtain pan-neuronal knockdown for select
610 homologs of 3q29 genes. For each RNAi line tested, groups of ten female flies were first
611 allowed to adjust at room temperature for 30 minutes and then transferred to a climbing
612 apparatus, made by joining two vials, and allowed to adjust for 5 minutes. The flies were
613 tapped down to the bottom, and the number of flies climbing past the 8 cm mark measured
614 from the bottom of the apparatus in 10 seconds was then counted (**S1 Video**, **S2 Video**). This
615 assay was repeated nine additional times for each group, with a one-minute rest between
616 trials. The sets of 10 trials for each group were repeated daily for ten days, capturing data for
617 100 replicates from day 1 until day 10, starting the experiments with 1-2-day old flies. All
618 experiments were performed during the same time of the day for consistency of results.

619

620 **Imaging of adult fly eyes and wings**

621 We crossed RNAi lines with *GMR-GAL4* and reared at 29°C for eye-specific knockdown and
622 *bx^{MS1096}-GAL4* at 25°C for wing-specific knockdown. For eye imaging, adult 2-3-day old
623 female progenies from the crosses were collected, immobilized by freezing at -80°C,
624 mounted on Blu-tac (Bostik Inc, Wauwatosa, WI, USA), and imaged with an Olympus BX53
625 compound microscope with LMPLan N 20X air objective using a DP73 c-mount camera at

626 0.5X magnification and a z-step size of 12.1 μ m. (Olympus Corporation, Tokyo, Japan). We
627 used CellSens Dimension software (Olympus Corporation, Tokyo, Japan) to capture the
628 images, and stacked the image slices using Zerene Stacker (Zerene Systems LLC, Richland,
629 WA, USA). All eye images presented in this study are maximum projections of 20
630 consecutive optical z-sections. Adult wings were plucked from 2-5 day old female flies,
631 mounted on a glass slide, covered with a coverslip and sealed with clear nail polish. The
632 wings were imaged using a Zeiss Discovery V20 stereoscope (Zeiss, Thornwood, NY, USA)
633 with ProgRes Speed XT Core 3 camera (Jenoptik AG, Jena, Germany) using a 40X objective,
634 and wing images were captured with ProgRes CapturePro v.2.8.8.

635

636 **Quantitative phenotyping of fly eyes using *Flynotyper***

637 We used a computational method called *Flynotyper* (<https://flynotyper.sourceforge.net>) to
638 measure the degree of roughness of the adult eyes with knockdown of individual or pairs of
639 homologs [53]. The software uses an algorithm to detect the center of each ommatidium, and
640 calculates a phenotypic score based on the number of ommatidia detected, the lengths of six
641 local vectors with direction pointing from each ommatidium to the neighboring ommatidia,
642 and the angle between these six local vectors (S2 Fig.). Eye areas, ommatidial diameter, and
643 areas of necrotic patches, which may not be reflected in the *Flynotyper* scores, were
644 measured using ImageJ [108]. Significant pairwise interactions were reported as “validated”
645 when multiple RNAi or mutant lines, if available, showed the same phenotype (S7 Table, S9
646 Table).

647

648 **Immunohistochemistry of eye and wing discs**

649 Third instar larval and 44-hour-old pupal eye discs, reared at 29°C, and third instar larval
650 wing discs, reared at 25°C, were dissected in 1X phosphate-buffered saline (PBS) and fixed
651 in 4% paraformaldehyde for 20 minutes. The eye and wing discs were then washed thrice in
652 PBT (PBS with 0.1% Triton-X) for 10 minutes each, treated with blocking solution (PBS
653 with 1% normal goat serum (NGS) for eye discs, or 1% bovine serum albumin (BSA) for
654 wing discs) for 30 minutes, and then incubated overnight with primary antibodies at 4°C.
655 Rabbit anti-cleaved *Drosophila* dcp1 (Asp216) (1:100; 9578S, Cell Signaling Technology,
656 Danvers, MA, USA), a marker for cells undergoing apoptosis, and Mouse anti-phospho-
657 Histone H3 (S10) antibody (1:100; 9706L, Cell Signaling Technology), a mitotic marker for
658 measuring proliferating cells, were used to assay cell proliferation and apoptosis defects in
659 larval eye and wing discs. Mouse anti-DLG (1:200; 4F3, DSHB, Iowa City, Iowa, USA), a

660 septate junction marker, and Rhodamine Phalloidin (1:200; R415, Invitrogen Molecular
661 Probes, Carlsbad, CA, USA), an F-actin marker, were used to visualize and count ommatidial
662 cells and photoreceptor cells in pupal eyes. Mouse anti-chaoptin (1:200; 24B10, DSHB) was
663 used to visualize retinal axon projections. Preparations were then washed thrice with PBT for
664 10 minutes, and incubated for two hours with fluorophore-conjugated secondary antibodies
665 (Alexa fluor 568 goat anti-mouse (1:200) (A11031), Alexa fluor 488 goat anti-mouse (1:200)
666 (A11029), Alexa fluor 647 goat anti-rabbit (1:200) (A21245), and Alexa fluor 647 goat anti-
667 mouse (1:200) (A21236), Invitrogen Molecular Probes, Carlsbad, CA, USA)) with gentle
668 shaking. Preparations were washed thrice in PBT for 10 minutes, and the tissues were then
669 mounted in Prolong Gold antifade mounting media with DAPI (P36930, Thermo Fisher
670 Scientific, Waltham, MA, USA) or Vectashield hard set mounting media with DAPI (H-
671 1500, Vector Laboratories, Burlingame, CA, USA) for imaging.

672

673 **Bromouridine staining**

674 Third instar larval eye discs were dissected in 1X PBS and immediately transferred to
675 Schneider's Insect Media (Sigma-Aldrich, St. Louis, MO). The tissues were then incubated in
676 10 µM BrdU (Sigma-Aldrich) at 25°C for one hour with constant agitation to allow for
677 incorporation of BrdU into DNA of replicating cells during the S-phase of cell cycle. The
678 samples were washed thrice with PBS for five minutes each and fixed in 4%
679 paraformaldehyde for 20 minutes. To denature DNA, the tissues were acid-treated in 2N HCl
680 for 20 minutes, neutralized in 100 mM Borax solution for 2 minutes, washed thrice in 10X
681 PBT (PBS with 0.1% Tween-20) for 10 minutes, and treated with blocking solution (PBS,
682 0.2% Triton X-100, 5% NGS) for one hour. The tissues were then incubated in mouse anti-
683 BrdU (1:200; G3G4, DSHB, Iowa City, Iowa, USA) and diluted in blocking solution
684 overnight at 4°C. The next day, the tissues were washed thrice in PBT for 20 minutes each
685 and incubated in Alexa fluor 568 goat anti-mouse (1:200, Invitrogen Molecular Probes,
686 Carlsbad, CA, USA) for two hours with constant agitation. Finally, the samples were
687 mounted in Prolong Gold antifade reagent with DAPI (Thermo Fisher Scientific, Waltham,
688 MA, USA) for imaging.

689

690 **Terminal deoxynucleotidyl transferase (TUNEL) Assay**

691 The levels of cell death in the developing eye were evaluated by staining using the *In Situ*
692 Cell Death Detection Kit, TMR Red (Roche, Basel, Switzerland). The third instar larval eye
693 discs were dissected in 1X PBS and fixed in 4% paraformaldehyde for 20 minutes at room

694 temperature, followed by three 10-minute washes with PBS. The dissected tissues were
695 permeabilized by treating with 20 µg/ml proteinase K (Sigma-Aldrich, St. Louis, MO, USA)
696 for two minutes, washed thrice in PBT (PBS with 0.1% Triton-X) for 5 minutes each, fixed in
697 4% paraformaldehyde for 15 minutes, and washed thrice again in PBT for 10 minutes each.
698 The tissues were then incubated overnight with TUNEL (terminal deoxynucleotidyl
699 transferase dUTP nick end labeling) reaction mixture at 4°C per the manufacturer's
700 instructions, and washed five times in PBT for 15 minutes each. Finally, tissues were
701 mounted in Prolong-gold antifade containing DAPI (Thermo Fisher Scientific, Waltham,
702 MA, USA) for imaging.

703

704 **Confocal imaging and analysis**

705 Confocal images of larval and pupal eye discs were captured using an Olympus Fluoview
706 FV1000 laser scanning confocal microscope (Olympus America, Lake Success,
707 NY). Maximum projections of all optical sections were generated for display. As DLG
708 staining was only used to visualize cell boundaries in the pupal eye and not for any
709 expression or quantitative analysis, we increased the laser intensity from 400-490V in
710 control flies to 530-570V in flies with knockdown of *dlg1* to account for decreased DLG
711 expression. Acquisition and processing of images was performed using the Fluoview
712 FV10-ASW 2.1 software (Olympus Corporation, Tokyo, Japan), and the z-stacks of images
713 were merged using ImageJ [108]. The number of pH3, BrdU, TUNEL, and dcp1-positive
714 cells from larval eye discs were counted using two ImageJ plugins, AnalyzeParticles and
715 Image-based Tool for Counting Nuclei (ITCN). As we found a strong correlation (Pearson
716 correlation, $r=0.736$, $p<2.2\times 10^{-16}$) between the two methods (**S2 Fig.**), all cell counts
717 displayed for eye data were derived from ITCN analysis. Proliferating cells in larval wing
718 discs stained with pH3 were counted using AnalyzeParticles, and apoptotic cells in wing
719 discs stained with dcp1 were analyzed using manual counting. Images stained with anti-
720 chaoptin were manually scored as having either “mild” (minor axon disorganization
721 compared with control), “moderate” (partial loss of axon projection. i.e. loss of R7-R8
722 projection into the medulla), or “severe” (loss of projections for most axons at the lamina)
723 axon targeting defects.

724

725 **Differential expression analysis of transcriptome data**

726 We performed RNA sequencing (RNA-Seq) of samples isolated from three biological
727 replicates of 35 fly heads each for individual (*Cbp20*, *dlg1*, *Fsn*, *Pak*) and pairwise

728 (*Cbp20/dlg1*, *Cbp20/Fsn*) *Elav-GAL4* mediated knockdowns of homologs of 3q29 genes. We
729 compared gene expression levels of each cross to VDRC control flies carrying the same
730 genetic background (GD or KK control lines crossed with *Elav-GAL4*). We prepared cDNA
731 libraries for the three biological replicates per genotype using TruSeq Stranded mRNA LT
732 Sample Prep Kit (Illumina, San Diego, CA), and performed single-end sequencing using
733 Illumina HiSeq 2000 at the Penn State Genomics Core Facility to obtain 100 bp reads at an
734 average coverage of 36.0 million aligned reads/sample. We used Trimmomatic v.0.36 [109]
735 for quality control assessment, TopHat2 v.2.1.1 [110] to align the raw sequencing data to the
736 reference fly genome and transcriptome (build 6.08), and HTSeq-Count v.0.6.1 [111] to
737 calculate raw read counts for each gene. edgeR v.3.20.1 [112] (generalized linear model
738 option) was used to perform differential expression analysis, and genes with \log_2 -fold
739 changes >1 or <-1 and false-discovery rates <0.05 (Benjamini-Hochberg correction) were
740 considered to be differentially expressed (**S3 File**). Human homologs of differentially-
741 expressed fly genes (top matches for each fly gene, excluding matches with “low” rank) were
742 identified using DIOPT [100]. Enrichment analysis of Panther GO-Slim Biological Process
743 terms among the differentially-expressed fly genes and their human homologs was performed
744 using the PantherDB Gene List Analysis tool [101]. Enrichments for genes preferentially
745 expressed in the developing brain were calculated using the Cell-type Specific Expression
746 Analysis tool [113] based on expression data from the BrainSpan Atlas [114].

747

748 ***X. laevis* embryos**

749 Eggs collected from female *X. laevis* frogs were fertilized *in vitro*, dejellied, and cultured
750 following standard methods [115,116]. Embryos were staged according to Nieuwkoop and
751 Faber [117]. All *X. laevis* experiments were approved by the Boston College Institutional
752 Animal Care and Use Committee (Protocol #2016-012) and were performed according to
753 national regulatory standards.

754

755 **Morpholino and RNA constructs**

756 Morpholinos (MOs) were targeted to early splice sites of *X. laevis ncgp2*, *fbxo45*, *pak2*, or
757 standard control MO, purchased from Gene Tools LLC (Philomath, OR, USA). MO
758 sequences are listed in **S12 Table**. For knockdown experiments, all MOs were injected at
759 either the 2-cell or 4-cell stage, with embryos receiving injections two or four times total in
760 0.1X MMR media containing 5% Ficoll. Control and *fbxo45* MOs were injected at
761 10ng/embryo, *ncgp2* and control MOs were injected at 20ng/embryo, and *pak2* and control

762 MOs were injected at 50ng/embryo. For rescue experiments (**S13 Fig.**), the same amounts of
763 MOs used in the KD experiments were injected along with gene-specific mRNA tagged with
764 GFP (800pg/embryo for *xiap*-GFP; 1000pg/embryo for *ncbp2*-GFP and *fbxo45*-GFP, and
765 300pg/embryo for *pak2*-GFP) in the same injection solution. Capped mRNAs were
766 transcribed *in vitro* using SP6 or T7 mMessage mMachine Kit (Thermo Fisher Scientific,
767 Waltham, MA, USA). RNA was purified with LiCl precipitation. *X. laevis* *ncbp2*, *fbxo45*,
768 *pak2*, and *xiap* ORFs obtained from the European *Xenopus* Resource Center (EXRC,
769 Portsmouth, UK) were gateway-cloned into pCSf107mT-GATEWAY-3'GFP destination
770 vectors. Constructs used included *ncbp2*-GFP, *fbxo45*-GFP, *pak2*-GFP, *xiap*-GFP, and GFP
771 in pCS2+. Embryos either at the 2-cell or 4-cell stage received four injections in 0.1X MMR
772 containing 5% Ficoll with the following total mRNA amount per embryo: 300pg of GFP,
773 800pg of *xiap*-GFP, 1000pg of *ncbp2*-GFP, 1000pg of *fbxo45*-GFP, and 300pg of *pak2*-GFP.
774

775 **qPCR for *X. laevis* morpholino knockdown**

776 Morpholino validation and knockdown was assessed using qPCR. Total RNA was extracted
777 using TRIzol reagent (Life Technologies, Grand Island, NY, USA), followed by chloroform
778 extraction and ethanol precipitation from 2-day old embryos injected with increasing
779 concentrations of MO targeted to each homolog of the tested 3q29 gene. cDNA synthesis was
780 performed with SuperScript II Reverse Transcriptase (Life Technologies, Grand Island, NY,
781 USA) and random hexamers. PCR primers are listed in **S13 Table**. qPCR was performed in
782 triplicate (**S12 Fig.**), with band intensities quantified by densitometry in ImageJ and
783 normalized to the uninjected control mean relative to *ODC1*, which was used as a
784 housekeeping control.
785

786 **Brain and eye morphology assays**

787 In brain morphology experiments, all embryos received two injections at the 2-cell stage in
788 0.1X MMR containing 5% Ficoll. One cell was left uninjected and the other cell was injected
789 with either control MO or MO targeted to the tested 3q29 gene, along with 300pg of GFP
790 mRNA in the same injection solution. Stage 47 tadpoles were fixed in 4% PFA diluted in
791 PBS for one hour, rinsed in PBS and gutted to reduce autofluorescence. Embryos were
792 incubated in 3% bovine serum albumin and 1% Triton-X 100 in PBS for two hours, and then
793 incubated in anti-acetylated tubulin primary antibody (1:500, monoclonal, clone 6-11B-1,
794 AB24610, Abcam, Cambridge, UK) and goat anti-mouse Alexa fluor 488 conjugate
795 secondary antibody (1:1000, polyclonal, A11029, Invitrogen Life Technologies, Carlsbad,

796 CA). Embryos were then rinsed in 1% PBS-Tween and imaged in PBS. Skin dorsal to the
797 brain was removed if the brain was not clearly visible due to pigment. For eye phenotype
798 experiments, all embryos received four injections at the 2-cell or 4-cell stage in 0.1X MMR
799 containing 5% Ficoll with either the control MO or MOs targeted to each 3q29 gene. Stage
800 42 tadpoles were fixed in 4% PFA diluted in PBS. Tadpoles were washed three times in 1%
801 PBS-Tween for one hour at room temperature before imaging.

802

803 ***X. laevis* image acquisition and analysis**

804 Lateral view images of stage 42 tadpoles for eye experiments and dorsal view images of state
805 47 tadpoles for brain experiments were each collected on a SteREO Discovery.V8
806 microscope using a Zeiss 5X objective and Axiocam 512 color camera (Zeiss, Thornwood,
807 NY, USA). Areas of the left and right eye, forebrain, and midbrain were determined from raw
808 images using the polygon area function in ImageJ. Eye size was quantified by taking the
809 average area of both the left and right eye, while forebrain and midbrain area were quantified
810 by taking the ratio between the injected and uninjected sides for each sample.

811

812 **Western blot for apoptosis**

813 Two replicate western blot experiments were performed to test for apoptosis markers in *X.*
814 *laevis* with 3q29 gene knockdown (**S12 Figure**). Embryos at stages 20-22 were lysed in
815 buffer (50mM Tris pH 7.5, 1% NP40, 150mM NaCl, 1mM PMSF, 0.5 mM EDTA)
816 supplemented with cOmplete Mini EDTA-free Protease Inhibitor Cocktail (Sigma-Aldrich,
817 Basel, Switzerland). Blotting was carried out using rabbit polyclonal antibody to cleaved
818 caspase-3 (1:500, 9661S, Cell Signaling Technology, Danvers, MA, USA), with mouse anti-
819 beta actin (1:2500, AB8224, Abcam, Cambridge, UK) as a loading control on a Mini-
820 PROTEAN TGX precast 4-15% gradient gel (Bio-Rad, Hercules, CA, USA).
821 Chemiluminescence detection was performed using Amersham ECL western blot reagent
822 (GE Healthcare Bio-Sciences, Pittsburgh, PA, USA). Band intensities were quantified by
823 densitometry in ImageJ and normalized to the control mean relative to beta-actin. Due to the
824 low number of replicates, we did not perform any statistical tests on data derived from these
825 experiments.

826

827 **Human brain-specific network analysis of 3q29 gene interactions**

828 We used a human brain-specific gene interaction network that was previously built using a
829 Bayesian classifier trained on gene co-expression datasets [56,57]. We extracted interactions

830 between pairs of genes with predicted weights >2.0 (containing the top 0.5% most likely
831 interactions) and measured the length of the shortest paths connecting pairs of 3q29 genes
832 within the network, excluding genes without connectivity in the network from final
833 calculations. As a control, we also measured the connectivity of 500 randomly selected genes
834 with 100 replicates each of 20 other random genes. All network analysis was performed using
835 the NetworkX Python package [118].

836

837 **Overlap between neurodevelopmental and apoptosis gene sets**

838 We obtained a set of 1,794 genes annotated with the Gene Ontology term for apoptotic
839 processes (GO:0006915) or children terms from the Gene Ontology Consortium (AmiGO
840 v.2.4.26) [119], and overlapped this gene set with sets of 756 candidate autism genes (SFARI
841 Gene Tiers 1-4) [77], 1,854 candidate intellectual disability genes [93], and 2,546 curated
842 candidate schizophrenia genes [76]. Genes in these three sets that were annotated for
843 apoptosis function are listed in **S4 File**. To determine the statistical significance of these
844 overlaps, we performed 100,000 simulations to identify the number of apoptosis genes among
845 groups of genes randomly selected from the genome, and determined the percentiles for each
846 observed overlap among the simulated overlaps as empirical p-values.

847

848 **Statistical analysis**

849 Details of each dataset and the associated statistical tests are provided in **S5 File**. All
850 statistical analyses of functional data were performed using R v.3.4.2 (R Foundation for
851 Statistical Computing, Vienna, Austria). Non-parametric one-tailed and two-tailed Mann-
852 Whitney tests were used to analyze *Drosophila* functional data and human network data, as
853 several datasets were not normally distributed ($p < 0.05$, Shapiro-Wilk tests for normality).
854 Climbing ability and survival data for each fly RNAi line across each experiment day were
855 analyzed using two-way and one-way repeated values ANOVA tests with post-hoc pairwise
856 t-tests. We also used parametric t-tests to analyze *Drosophila* qPCR data and all *X. laevis*
857 data, as these data were either normally distributed ($p > 0.05$, Shapiro-Wilk tests for normality)
858 or had a robust sample size ($n > 30$) for non-normality. All p-values from statistical tests
859 derived from similar sets of experiments (i.e. *Flynotyper* scores for pairwise interactions,
860 dcp1 rescue experiments with *Diap1*) were corrected using Benjamini-Hochberg correction.

861

862

863

864 **Reproducibility**

865 *Drosophila* eye area and pH3 and TUNEL staining experiments for select individual
866 knockdown lines, as well as climbing ability experiments for a subset of individual and
867 pairwise knockdown lines, were performed on two independent occasions with similar
868 sample sizes. Data displayed in the main figures were derived from single batches, while data
869 from the repeated experiments are shown in **S14 Fig.** *X. laevis* brain and eye area
870 experiments were performed on three independent occasions, with the data shown in the
871 figures representing pooled results of each of the three experimental batches (normalized to
872 the respective controls from each batch). *X. laevis* qPCR experiments were performed three
873 times and western blot experiments were performed twice, with the blots/gels for each
874 replicate experiment shown in **S12 Fig.** Sample sizes for each experiment were determined
875 by testing all available organisms; no prior power calculations for sample size estimation
876 were performed. No data points or outliers were excluded from the experiments presented in
877 the manuscript.

878

879 **Data availability**

880 Gene expression data for the six *Drosophila* individual and pairwise RNAi knockdown of
881 homologs of 3q29 genes are deposited in the GEO (Gene Expression Omnibus) database with
882 accession code GSE128094, and the raw RNA Sequencing files are deposited in the SRA
883 (Sequence Read Archive) with BioProject accession PRJNA526450. All other data generated
884 and analyzed in study are included in the manuscript and supporting files. All unique
885 biological materials described in the manuscript, such as recombined fly stocks, are readily
886 available from the authors upon request.

887

888 **Code availability**

889 All source code and datasets for generating genomic data (RNA-Seq, network analysis, and
890 neurodevelopment/apoptosis gene overlap) are available on the Girirajan lab GitHub page at
891 https://github.com/girirajanlab/3q29_project.

892

893 **ACKNOWLEDGMENTS**

894 We thank A. Krishnan for assistance with the brain-specific gene interaction network
895 analysis, J. Tiber for technical assistance with the *X. laevis* experiments, and V. Faundez
896 for useful discussions and critical reading of the manuscript.

897 **REFERENCES**

- 898 1. Malhotra D, Sebat J. CNVs: Harbingers of a rare variant revolution in psychiatric
899 genetics. *Cell*. 2012;148: 1223–1241. doi:10.1016/j.cell.2012.02.039
- 900 2. Girirajan S, Campbell CD, Eichler EE. Human Copy Number Variation and Complex
901 Genetic Disease. *Annu Rev Genet*. 2011;45: 203–226. doi:10.1146/annurev-genet-
902 102209-163544
- 903 3. Girirajan S, Eichler EE. Phenotypic variability and genetic susceptibility to genomic
904 disorders. *Hum Mol Genet*. 2010;19: R176-87. doi:10.1093/hmg/ddq366
- 905 4. Karayiorgou M, Morris MA, Morrow B, Shprintzen RJ, Goldberg R, Borrow J, et al.
906 Schizophrenia susceptibility associated with interstitial deletions of chromosome
907 22q11. *Proc Natl Acad Sci U S A*. 1995;92: 7612–7616. doi:10.1073/pnas.92.17.7612
- 908 5. Karayiorgou M, Simon TJ, Gogos JA. 22q11.2 microdeletions: Linking DNA
909 structural variation to brain dysfunction and schizophrenia. *Nat Rev Neurosci*.
910 2010;11: 402–416. doi:10.1038/nrn2841
- 911 6. Fenelon K, Mukai J, Xu B, Hsu P-K, Drew LJ, Karayiorgou M, et al. Deficiency of
912 Dgcr8, a gene disrupted by the 22q11.2 microdeletion, results in altered short-term
913 plasticity in the prefrontal cortex. *Proc Natl Acad Sci U S A*. 2011;108: 4447–4452.
914 doi:10.1073/pnas.1101219108
- 915 7. Mukai J, Tamura M, Fénelon K, Rosen AM, Spellman TJ, Kang R, et al. Molecular
916 substrates of altered axonal growth and brain connectivity in a mouse model of
917 schizophrenia. *Neuron*. 2015;86: 680–95. doi:10.1016/j.neuron.2015.04.003
- 918 8. Ballif BC, Theisen A, Coppinger J, Gowans GC, Hersh JH, Madan-Khetarpal S, et al.
919 Expanding the clinical phenotype of the 3q29 microdeletion syndrome and
920 characterization of the reciprocal microduplication. *Mol Cytogenet*. 2008;1: 8.
921 doi:10.1186/1755-8166-1-8
- 922 9. Mulle JG, Dodd AF, McGrath JA, Wolyniec PS, Mitchell AA, Shetty AC, et al.
923 Microdeletions of 3q29 confer high risk for schizophrenia. *Am J Hum Genet*. 2010;87:
924 229–236. doi:10.1016/j.ajhg.2010.07.013
- 925 10. Glassford MR, Rosenfeld JA, Freedman AA, Zwick ME, Mulle JG. Novel features of
926 3q29 deletion syndrome: Results from the 3q29 registry. *Am J Med Genet Part A*.
927 2016;170: 999–1006. doi:10.1002/ajmg.a.37537
- 928 11. Kirov G, Pocklington AJ, Holmans P, Ivanov D, Ikeda M, Ruderfer D, et al. De novo
929 CNV analysis implicates specific abnormalities of postsynaptic signalling complexes
930 in the pathogenesis of schizophrenia. *Mol Psychiatry*. 2012;17: 142–153.
931 doi:10.1038/mp.2011.154
- 932 12. Mulle JG. The 3q29 deletion confers >40-fold increase in risk for schizophrenia. *Mol
933 Psychiatry*. 2015;20: 1028–1029. doi:10.1038/mp.2015.76
- 934 13. Pollak RM, Murphy MM, Epstein MP, Zwick ME, Klaiman C, Saulnier CA, et al.
935 Neuropsychiatric phenotypes and a distinct constellation of ASD features in 3q29
936 deletion syndrome: results from the 3q29 registry. *Mol Autism*. 2019;10: 30.
937 doi:10.1186/s13229-019-0281-5

938 14. Rutkowski TP, Purcell RH, Pollak RM, Grewenow SM, Gafford GM, Malone T, et al.
939 Behavioral changes and growth deficits in a CRISPR engineered mouse model of the
940 schizophrenia-associated 3q29 deletion. *Mol Psychiatry*. 2019. doi:10.1038/s41380-
941 019-0413-5

942 15. Baba M, Yokoyama K, Seiriki K, Naka Y, Matsumura K, Kondo M, et al. Psychiatric-
943 disorder-related behavioral phenotypes and cortical hyperactivity in a mouse model of
944 3q29 deletion syndrome. *Neuropsychopharmacology*. 2019;44: 2125–2135.
945 doi:10.1038/s41386-019-0441-5

946 16. Quintero-Rivera F, Sharifi-Hannauer P, Martinez-Agosto JA. Autistic and psychiatric
947 findings associated with the 3q29 microdeletion syndrome: Case report and review.
948 *Am J Med Genet Part A*. 2010;152 A: 2459–2467. doi:10.1002/ajmg.a.33573

949 17. Rutkowski TP, Schroeder JP, Gafford GM, Warren ST, Weinshenker D, Caspary T, et
950 al. Unraveling the genetic architecture of copy number variants associated with
951 schizophrenia and other neuropsychiatric disorders. *J Neurosci Res*. 2017;95: 1144–
952 1160. doi:10.1002/jnr.23970

953 18. Budnik V, Koh YH, Guan B, Hartmann B, Hough C, Woods D, et al. Regulation of
954 synapse structure and function by the *Drosophila* tumor suppressor gene *dlg*. *Neuron*.
955 1996;17: 627–640. doi:10.1016/S0896-6273(00)80196-8

956 19. Walch L. Emerging role of the scaffolding protein Dlg1 in vesicle trafficking. *Traffic*.
957 2013;14: 964–973. doi:10.1111/tra.12089

958 20. Andrews T, Meader S, Vulto-van Silfhout A, Taylor A, Steinberg J, Hehir-Kwa J, et
959 al. Gene Networks Underlying Convergent and Pleiotropic Phenotypes in a Large and
960 Systematically-Phenotyped Cohort with Heterogeneous Developmental Disorders.
961 *PLoS Genet*. 2015;11: e1005012. doi:10.1371/journal.pgen.1005012

962 21. Iyer J, Singh MD, Jensen M, Patel P, Pizzo L, Huber E, et al. Pervasive genetic
963 interactions modulate neurodevelopmental defects of the autism-associated 16p11.2
964 deletion in *Drosophila melanogaster*. *Nat Commun*. 2018;9: 2548.
965 doi:10.1038/s41467-018-04882-6

966 22. Jensen M, Girirajan S. An interaction-based model for neuropsychiatric features of
967 copy-number variants. *PLoS Genet*. 2019;15: e1007879.
968 doi:10.1371/journal.pgen.1007879

969 23. Wangler MF, Yamamoto S, Bellen HJ. Fruit flies in biomedical research. *Genetics*.
970 2015;199: 639–653. doi:10.1534/genetics.114.171785

971 24. Pratt KG, Khakhlin AS. Modeling human neurodevelopmental disorders in the
972 *Xenopus* tadpole: from mechanisms to therapeutic targets. *Dis Model Mech*. 2013;6:
973 1057–1065. doi:10.1242/dmm.012138

974 25. Reiter LT, Potocki L, Chien S, Gribskov M, Bier E. A systematic analysis of human
975 disease-associated gene sequences in *Drosophila melanogaster*. *Genome Res*. 2001;11:
976 1114–1125. doi:10.1101/gr.169101

977 26. Gatto CL, Broadie K. Drosophila modeling of heritable neurodevelopmental disorders.
978 *Curr Opin Neurobiol*. 2011;21: 834–841. doi:10.1016/j.conb.2011.04.009

979 27. Harland RM, Grainger RM. Xenopus research: Metamorphosed by genetics and
980 genomics. *Trends Genet.* 2011;27: 507–515. doi:10.1016/j.tig.2011.08.003

981 28. Dickman DK, Davis GW. The schizophrenia susceptibility gene dysbindin controls
982 synaptic homeostasis. *Science*). 2009;326: 1127–1130. doi:10.1126/science.1179685

983 29. Shao L, Shuai Y, Wang J, Feng S, Lu B, Li Z, et al. Schizophrenia susceptibility gene
984 dysbindin regulates glutamatergic and dopaminergic functions via distinctive
985 mechanisms in *Drosophila*. *Proc Natl Acad Sci U S A.* 2011;108: 18831–18836.
986 doi:10.1073/pnas.1114569108

987 30. Wu Y, Bolduc F V., Bell K, Tully T, Fang Y, Sehgal A, et al. A *Drosophila* model for
988 Angelman syndrome. *Proc Natl Acad Sci U S A.* 2008;105: 12399–12404.
989 doi:10.1073/pnas.0805291105

990 31. Marshak S, Meynard MM, de Vries YA, Kidane AH, Cohen-Cory S. Cell-autonomous
991 alterations in dendritic arbor morphology and connectivity induced by overexpression
992 of MeCP2 in *Xenopus* central neurons in vivo. *PLoS One.* 2012;7: e33153.
993 doi:10.1371/journal.pone.0033153

994 32. Muller BM, Kistner U, Veh RW, Cases-Langhoff C, Becker B, Gundelfinger ED, et al.
995 Molecular characterization and spatial distribution of SAP97, a novel presynaptic
996 protein homologous to SAP90 and the *Drosophila* discs-large tumor suppressor
997 protein. *J Neurosci.* 1995;15: 2354–2366. doi:10.1523/jneurosci.15-03-02354.1995

998 33. Sabin LR, Zhou R, Gruber JJ, Lukinova N, Bambina S, Berman A, et al. Ars2
999 Regulates Both miRNA- and siRNA- Dependent Silencing and Suppresses RNA Virus
1000 Infection in *Drosophila*. *Cell.* 2009;138: 340–351. doi:10.1016/j.cell.2009.04.045

1001 34. Brand AH, Perrimon N. Targeted gene expression as a means of altering cell fates and
1002 generating dominant phenotypes. *Development.* 1993;118: 401–415.

1003 35. Thomas U, Kim E, Kuhlendahl S, Koh YH, Gundelfinger ED, Sheng M, et al.
1004 Synaptic clustering of the cell adhesion molecule Fasciclin II by discs- large and its
1005 role in the regulation of presynaptic structure. *Neuron.* 1997;19: 787–799.
1006 doi:10.1016/S0896-6273(00)80961-7

1007 36. Armstrong JD, Texada MJ, Munjaal R, Baker DA, Beckingham KM. Gravitaxis in
1008 *Drosophila melanogaster*: A forward genetic screen. *Genes, Brain Behav.* 2006;5:
1009 222–239. doi:10.1111/j.1601-183X.2005.00154.x

1010 37. Mendoza-Topaz C, Urra F, Barria R, Albornoz V, Ugalde D, Thomas U, et al.
1011 DLGS97/SAP97 is developmentally upregulated and is required for complex adult
1012 behaviors and synapse morphology and function. *J Neurosci.* 2008;28: 304–314.
1013 doi:10.1523/JNEUROSCI.4395-07.2008

1014 38. Hing H, Xiao J, Harden N, Lim L, Lawrence Zipursky S. Pak functions downstream of
1015 Dock to regulate photoreceptor axon guidance in *Drosophila*. *Cell.* 1999;97: 853–863.
1016 doi:10.1016/S0092-8674(00)80798-9

1017 39. Kim MD, Kamiyama D, Kolodziej P, Hing H, Chiba A. Isolation of Rho GTPase
1018 effector pathways during axon development. *Dev Biol.* 2003;262: 282–293.
1019 doi:10.1016/S0012-1606(03)00393-2

1020 40. Parnas D, Haghghi AP, Fetter RD, Kim SW, Goodman CS. Regulation of
1021 postsynaptic structure and protein localization by the Rho-type guanine nucleotide
1022 exchange factor dPix. *Neuron*. 2001;32: 415–424. doi:10.1016/S0896-6273(01)00485-
1023 8

1024 41. Ng J, Luo L. Rho GTPases regulate axon growth through convergent and divergent
1025 signaling pathways. *Neuron*. 2004;44: 779–793. doi:10.1016/j.neuron.2004.11.014

1026 42. Sherwood NT, Sun Q, Xue M, Zhang B, Zinn K. Drosophila spastin regulates synaptic
1027 microtubule networks and is required for normal motor function. *PLoS Biol*. 2004;2:
1028 e429. doi:10.1371/journal.pbio.0020429

1029 43. Chen SY, Huang PH, Cheng HJ. Disrupted-in-schizophrenia 1-mediated axon
1030 guidance involves TRIO-RAC-PAK small GTPase pathway signaling. *Proc Natl Acad
1031 Sci U S A*. 2011;108: 5861–5866. doi:10.1073/pnas.1018128108

1032 44. Morales J, Hiesinger PR, Schroeder AJ, Kume K, Verstreken P, Jackson FR, et al.
1033 Drosophila fragile X protein DFXR regulates neuronal morphology and function in the
1034 brain. *Neuron*. 2002;34: 961–972. doi:10.1016/S0896-6273(02)00731-6

1035 45. Thomas BJ, Wassarman DA. A fly's eye view of biology. *Trends Genet*. 1999;15:
1036 184–190. doi:10.1016/S0168-9525(99)01720-5

1037 46. Thaker HM, Kankel DR. Mosaic analysis gives an estimate of the extent of genomic
1038 involvement in the development of the visual system in *Drosophila melanogaster*.
1039 *Genetics*. 1992;131: 883–894.

1040 47. Oortveld MAW, Keerthikumar S, Oti M, Nijhof B, Fernandes AC, Kochinke K, et al.
1041 Human Intellectual Disability Genes Form Conserved Functional Modules in
1042 *Drosophila*. *PLoS Genet*. 2013;9: e1003911. doi:10.1371/journal.pgen.1003911

1043 48. Cukier HN, Perez AM, Collins AL, Zhou Z, Zoghbi HY, Botas J. Genetic modifiers of
1044 MeCP2 function in *Drosophila*. *PLoS Genet*. 2008;4: e1000179.
1045 doi:10.1371/journal.pgen.1000179

1046 49. Bilen J, Bonini NM. Genome-wide screen for modifiers of ataxin-3 neurodegeneration
1047 in *Drosophila*. *PLoS Genet*. 2007;3: 1950–64. doi:10.1371/journal.pgen.0030177

1048 50. Neufeld TP, Tang AH, Rubin GM. A genetic screen to identify components of the sina
1049 signaling pathway in *Drosophila* eye development. *Genetics*. 1998;148: 277–286.

1050 51. Cagan RL, Ready DF. The emergence of order in the *Drosophila* pupal retina. *Dev
1051 Biol*. 1989;136: 346–362. doi:10.1016/0012-1606(89)90261-3

1052 52. Kumar JP. Building an ommatidium one cell at a time. *Dev Dyn*. 2012;241: 136–149.
1053 doi:10.1002/dvdy.23707

1054 53. Iyer J, Wang Q, Le T, Pizzo L, Grönke S, Ambegaokar SS, et al. Quantitative
1055 assessment of eye phenotypes for functional genetic studies using *Drosophila*
1056 *melanogaster*. *G3 Genes, Genomes, Genet*. 2016;6: 1427–1437.
1057 doi:10.1534/g3.116.027060

1058 54. Grice SJ, Liu J-L, Webber C. Synergistic Interactions between *Drosophila* Orthologues
1059 of Genes Spanned by De Novo Human CNVs Support Multiple-Hit Models of Autism.

1060 PLOS Genet. 2015;11: e1004998. doi:10.1371/journal.pgen.1004998

1061 55. Warde-Farley D, Donaldson SL, Comes O, Zuberi K, Badrawi R, Chao P, et al. The
1062 GeneMANIA prediction server: Biological network integration for gene prioritization
1063 and predicting gene function. Nucleic Acids Res. 2010;38: W214-20.
1064 doi:10.1093/nar/gkq537

1065 56. Greene CS, Krishnan A, Wong AK, Ricciotti E, Zelaya RA, Himmelstein DS, et al.
1066 Understanding multicellular function and disease with human tissue-specific networks.
1067 Nat Genet. 2015;47: 569–576. doi:10.1038/ng.3259

1068 57. Krishnan A, Zhang R, Yao V, Theesfeld CL, Wong AK, Tadych A, et al. Genome-
1069 wide prediction and functional characterization of the genetic basis of autism spectrum
1070 disorder. Nat Neurosci. 2016;19: 1454–1462. doi:10.1038/nn.4353

1071 58. Paterlini M, Zakharenko SS, Lai WS, Qin J, Zhang H, Mukai J, et al. Transcriptional
1072 and behavioral interaction between 22q11.2 orthologs modulates schizophrenia-related
1073 phenotypes in mice. Nat Neurosci. 2005;8: 1586–1594. doi:10.1038/nn1562

1074 59. Yamaguchi Y, Miura M. Programmed Cell Death in Neurodevelopment. Dev Cell.
1075 2015;32: 478–490. doi:10.1016/j.devcel.2015.01.019

1076 60. Ernst C. Proliferation and Differentiation Deficits are a Major Convergence Point for
1077 Neurodevelopmental Disorders. Trends Neurosci. 2016;39: 290–299.
1078 doi:10.1016/j.tins.2016.03.001

1079 61. Pinto D, Pagnamenta AT, Klei L, Anney R, Merico D, Regan R, et al. Functional
1080 impact of global rare copy number variation in autism spectrum disorders. Nature.
1081 2010;466: 368–372. doi:10.1038/nature09146

1082 62. Glantz LA, Gilmore JH, Lieberman JA, Jarskog LF. Apoptotic mechanisms and the
1083 synaptic pathology of schizophrenia. Schizophr Res. 2006;81: 47–63.
1084 doi:10.1016/j.schres.2005.08.014

1085 63. Steller H. Regulation of apoptosis in Drosophila. Cell Death Differ. 2008;15: 1132–
1086 1138. doi:10.1038/cdd.2008.50

1087 64. Coe BP, Girirajan S, Eichler EE. A genetic model for neurodevelopmental disease.
1088 Curr Opin Neurobiol. 2012;22: 829–836. doi:10.1016/j.conb.2012.04.007

1089 65. Nicholas AK, Swanson EA, Cox JJ, Karbani G, Malik S, Springell K, et al. The
1090 molecular landscape of ASPM mutations in primary microcephaly. J Med Genet.
1091 2009;46: 249–253. doi:10.1136/jmg.2008.062380

1092 66. Coba MP, Ramaker MJ, Ho E V, Thompson SL, Komiyama NH, Grant SGN, et al.
1093 Dlgap1 knockout mice exhibit alterations of the postsynaptic density and selective
1094 reductions in sociability. Sci Rep. 2018;8: 2281. doi:10.1038/s41598-018-20610-y

1095 67. Duffney LJ, Zhong P, Wei J, Matas E, Cheng J, Qin L, et al. Autism-like Deficits in
1096 Shank3-Deficient Mice Are Rescued by Targeting Actin Regulators. Cell Rep.
1097 2015;11: 1400–1413. doi:10.1016/j.celrep.2015.04.064

1098 68. Park E, Na M, Choi J, Kim S, Lee J-R, Yoon J, et al. The Shank Family of
1099 Postsynaptic Density Proteins Interacts with and Promotes Synaptic Accumulation of

1100 the β PIX Guanine Nucleotide Exchange Factor for Rac1 and Cdc42. *J Biol Chem.*
1101 2003;278: 19220–19229. doi:10.1074/jbc.M301052200

1102 69. Saiga T, Fukuda T, Matsumoto M, Tada H, Okano HJ, Okano H, et al. Fbxo45 Forms
1103 a Novel Ubiquitin Ligase Complex and Is Required for Neuronal Development. *Mol*
1104 *Cell Biol.* 2009;29: 3529–3543. doi:10.1128/mcb.00364-09

1105 70. Marlin JW, Chang YWE, Ober M, Handy A, Xu W, Jakobi R. Functional PAK-2
1106 knockout and replacement with a caspase cleavage-deficient mutant in mice reveals
1107 differential requirements of full-length PAK-2 and caspase-activated PAK-2p34.
1108 *Mamm Genome.* 2011;22: 306–317. doi:10.1007/s00335-011-9326-6

1109 71. Wang L, Magdaleno S, Tabas I, Jackowski S. Early Embryonic Lethality in Mice with
1110 Targeted Deletion of the CTP:Phosphocholine Cytidyltransferase Gene (Pcyt1a).
1111 *Mol Cell Biol.* 2005;25: 3357–3363. doi:10.1128/mcb.25.8.3357-3363.2005

1112 72. Wang Y, Zeng C, Li J, Zhou Z, Ju X, Xia S, et al. PAK2 Haploinsufficiency Results in
1113 Synaptic Cytoskeleton Impairment and Autism-Related Behavior. *Cell Rep.* 2018;24:
1114 2029–2041. doi:10.1016/j.celrep.2018.07.061

1115 73. Levy JE, Jin O, Fujiwara Y, Kuo F, Andrews NC. Transferrin receptor is necessary for
1116 development of erythrocytes and the nervous system. *Nat Genet.* 1999;21: 396–399.
1117 doi:10.1038/7727

1118 74. Eicher JD, Landowski C, Stackhouse B, Sloan A, Chen W, Jensen N, et al. GRASP
1119 v2.0: An update on the Genome-Wide Repository of Associations between SNPs and
1120 Phenotypes. *Nucleic Acids Res.* 2015;43: D799–D804. doi:10.1093/nar/gku1202

1121 75. Turner TN, Yi Q, Krumm N, Huddleston J, Hoekzema K, Stessman HAF, et al. NAR
1122 Breakthrough Article denovo-db: A compendium of human de novo variants. *Nucleic*
1123 *Acids Res.* 2017;45: D804–D811. doi:10.1093/nar/gkw865

1124 76. Purcell SM, Moran JL, Fromer M, Ruderfer D, Solovieff N, Roussos P, et al. A
1125 polygenic burden of rare disruptive mutations in schizophrenia. *Nature.* 2014;506:
1126 185–190. doi:10.1038/nature12975

1127 77. Abrahams BS, Arking DE, Campbell DB, Mefford HC, Morrow EM, Weiss LA, et al.
1128 SFARI Gene 2.0: A community-driven knowledgebase for the autism spectrum
1129 disorders (ASDs). *Mol Autism.* 2013;4: 36. doi:10.1186/2040-2392-4-36

1130 78. Pabis M, Neufeld N, Shav-Tal Y, Neugebauer KM. Binding properties and dynamic
1131 localization of an alternative isoform of the cap-binding complex subunit CBP20.
1132 *Nucleus.* 2010;1: 412–21. doi:10.4161/nucl.1.5.12839

1133 79. Maquat LE. Nonsense-mediated mRNA decay: Splicing, translation and mRNP
1134 dynamics. *Nat Rev Mol Cell Biol.* 2004;5: 89–99. doi:10.1038/nrm1310

1135 80. Gonatopoulos-Pournatzis T, Cowling VH. Cap-binding complex (CBC). *Biochem J.*
1136 2014;458: 185–185. doi:10.1042/bj4580185

1137 81. Xu D, Woodfield SE, Lee T V, Fan Y, Antonio C, Bergmann A. Genetic control of
1138 programmed cell death (apoptosis) in *Drosophila*. *Fly (Austin).* 2009;3: 78–90.
1139 doi:10.4161/fly.3.1.7800

1140 82. Kornbluth S, White K. Apoptosis in Drosophila: Neither fish nor fowl (nor man, nor
1141 worm). *J Cell Sci.* 2005;118: 1779–1787. doi:10.1242/jcs.02377

1142 83. Tittel JN, Steller H. A comparison of programmed cell death between species. *Genome
1143 Biol.* 2000;1: REVIEWS0003. doi:10.1186/gb-2000-1-3-reviews0003

1144 84. Bilder D, Li M, Perrimon N. Cooperative regulation of cell polarity and growth by
1145 Drosophila tumor suppressors. *Science.* 2000;289: 113–116.
1146 doi:10.1126/science.289.5476.113

1147 85. Humbert P, Russell S, Richardson H. Dlg, scribble and Lgl in cell polarity, cell
1148 proliferation and cancer. *BioEssays.* 2003;25: 542–553. doi:10.1002/bies.10286

1149 86. Shin EY, Shin KS, Lee CS, Woo KN, Quan SH, Soung NK, et al. Phosphorylation of
1150 p85 β PIX, a Rac/Cdc42-specific guanine nucleotide exchange factor, via the
1151 Ras/ERK/PAK2 pathway is required for basic fibroblast growth factor-induced neurite
1152 outgrowth. *J Biol Chem.* 2002;277: 44417–44430. doi:10.1074/jbc.M203754200

1153 87. Luo S, Rubinsztein DC. Huntington promotes cell survival by preventing Pak2
1154 cleavage. *J Cell Sci.* 2009;122: 875–885. doi:10.1242/jcs.050013

1155 88. Courchesne E, Mouton PR, Calhoun ME, Semendeferi K, Ahrens-Barbeau C, Hallet
1156 MJ, et al. Neuron number and size in prefrontal cortex of children with autism. *JAMA
1157 - J Am Med Assoc.* 2011;306: 2001–2010. doi:10.1001/jama.2011.1638

1158 89. Kreczmanski P, Heinsen H, Mantua V, Woltersdorf F, Masson T, Ulfhake N, et al.
1159 Volume, neuron density and total neuron number in five subcortical regions in
1160 schizophrenia. *Brain.* 2007;130: 678–692. doi:10.1093/brain/awl386

1161 90. Dong D, Zielke HR, Yeh D, Yang P. Cellular stress and apoptosis contribute to the
1162 pathogenesis of autism spectrum disorder. *Autism Res.* 2018;11: 1076–1090.
1163 doi:10.1002/aur.1966

1164 91. Batalla A, Bargalló N, Gassó P, Molina O, Pareto D, Mas S, et al. Apoptotic markers
1165 in cultured fibroblasts correlate with brain metabolites and regional brain volume in
1166 antipsychotic-naïve first-episode schizophrenia and healthy controls. *Transl
1167 Psychiatry.* 2015;5: e626. doi:10.1038/tp.2015.122

1168 92. Gassó P, Mas S, Molina O, Lafuente A, Bernardo M, Parellada E. Increased
1169 susceptibility to apoptosis in cultured fibroblasts from antipsychotic-naïve first-episode
1170 schizophrenia patients. *J Psychiatr Res.* 2014;48: 94–101.
1171 doi:10.1016/j.jpsychires.2013.09.017

1172 93. Thormann A, Halachev M, McLaren W, Moore DJ, Svinti V, Campbell A, et al.
1173 Flexible and scalable diagnostic filtering of genomic variants using G2P with Ensembl
1174 VEP. *Nat Commun.* 2019;10: 2373. doi:10.1038/s41467-019-10016-3

1175 94. Girirajan S, Rosenfeld JA, Coe BP, Parikh S, Friedman N, Goldstein A, et al.
1176 Phenotypic Heterogeneity of Genomic Disorders and Rare Copy-Number Variants. *N
1177 Engl J Med.* 2012;367: 1321–1331. doi:10.1056/NEJMoa1200395

1178 95. Lindsay EA, Vitelli F, Su H, Morishima M, Huynh T, Prampano T, et al. Tbx1
1179 haploinsufficiency in the DiGeorge syndrome region causes aortic arch defects in
1180 mice. *Nature.* 2001;410: 97–101. doi:10.1038/35065105

1181 96. Poulton CJ, Schot R, Kia SK, Jones M, Verheijen FW, Venselaar H, et al.
1182 Microcephaly with simplified gyration, epilepsy, and infantile diabetes linked to
1183 inappropriate apoptosis of neural progenitors. *Am J Hum Genet.* 2011;89: 265–276.
1184 doi:10.1016/j.ajhg.2011.07.006

1185 97. Silver DL, Watkins-Chow DE, Schreck KC, Pierfelice TJ, Larson DM, Burnetti AJ, et
1186 al. The exon junction complex component Magoh controls brain size by regulating
1187 neural stem cell division. *Nat Neurosci.* 2010;13: 551–558. doi:10.1038/nn.2527

1188 98. Faheem M, Naseer MI, Rasool M, Chaudhary AG, Kumosani TA, Ilyas AM, et al.
1189 Molecular genetics of human primary microcephaly: an overview. *BMC Med
1190 Genomics.* 2015;8: S4. doi:10.1186/1755-8794-8-S1-S4

1191 99. Frappart P-O, Tong W-M, Demuth I, Radovanovic I, Herceg Z, Aguzzi A, et al. An
1192 essential function for NBS1 in the prevention of ataxia and cerebellar defects. *Nat
1193 Med.* 2005;11: 538–544. doi:10.1038/nm1228

1194 100. Hu Y, Flockhart I, Vinayagam A, Bergwitz C, Berger B, Perrimon N, et al. An
1195 integrative approach to ortholog prediction for disease-focused and other functional
1196 studies. *BMC Bioinformatics.* 2011;12: 357. doi:10.1186/1471-2105-12-357

1197 101. Mi H, Huang X, Muruganujan A, Tang H, Mills C, Kang D, et al. PANTHER version
1198 11: expanded annotation data from Gene Ontology and Reactome pathways, and data
1199 analysis tool enhancements. *Nucleic Acids Res.* 2017;45: D183–D189.
1200 doi:10.1093/nar/gkw1138

1201 102. Dietzl G, Chen D, Schnorrer F, Su K-C, Barinova Y, Fellner M, et al. A genome-wide
1202 transgenic RNAi library for conditional gene inactivation in *Drosophila*. *Nature.*
1203 2007;448: 151–6. doi:10.1038/nature05954

1204 103. Green EW, Fedele G, Giorgini F, Kyriacou CP. A *Drosophila* RNAi collection is
1205 subject to dominant phenotypic effects. *Nat Methods.* 2014;11: 222–223.
1206 doi:10.1038/nmeth.2856

1207 104. Chintapalli VR, Wang J, Dow JAT. Using FlyAtlas to identify better *Drosophila*
1208 melanogaster models of human disease. *Nat Genet.* 2007;39: 715–720.
1209 doi:10.1038/ng2049

1210 105. Graveley BR, Brooks AN, Carlson JW, Duff MO, Landolin JM, Yang L, et al. The
1211 developmental transcriptome of *Drosophila melanogaster*. *Nature.* 2011;471: 473–479.
1212 doi:10.1038/nature09715

1213 106. Ye J, Coulouris G, Zaretskaya I, Cutcutache I, Rozen S, Madden TL. Primer-BLAST:
1214 A tool to design target-specific primers for polymerase chain reaction. *BMC
1215 Bioinformatics.* 2012;13: 134. doi:10.1186/1471-2105-13-134

1216 107. Livak KJ, Schmittgen TD. Analysis of Relative Gene Expression Data Using Real-
1217 Time Quantitative PCR and the $2^{-\Delta\Delta CT}$ Method. *Methods.* 2001;25: 402–408.
1218 doi:10.1006/meth.2001.1262

1219 108. Schneider CA, Rasband WS, Eliceiri KW. NIH Image to ImageJ: 25 years of image
1220 analysis. *Nat Methods.* 2012;9: 671–675. doi:10.1038/nmeth.2089

1221 109. Bolger AM, Lohse M, Usadel B. Trimmomatic: A flexible trimmer for Illumina

1222 sequence data. *Bioinformatics*. 2014;30: 2114–2120.
1223 doi:10.1093/bioinformatics/btu170

1224 110. Kim D, Pertea G, Trapnell C, Pimentel H, Kelley R, Salzberg SL. TopHat2: accurate
1225 alignment of transcriptomes in the presence of insertions, deletions and gene fusions.
1226 *Genome Biol.* 2013;14: R36. doi:10.1186/gb-2013-14-4-r36

1227 111. Anders S, Pyl PT, Huber W. HTSeq-A Python framework to work with high-
1228 throughput sequencing data. *Bioinformatics*. 2015;31: 166–169.
1229 doi:10.1093/bioinformatics/btu638

1230 112. Robinson MD, McCarthy DJ, Smyth GK. edgeR: A Bioconductor package for
1231 differential expression analysis of digital gene expression data. *Bioinformatics*.
1232 2009;26: 139–140. doi:10.1093/bioinformatics/btp616

1233 113. Dougherty JD, Schmidt EF, Nakajima M, Heintz N. Analytical approaches to RNA
1234 profiling data for the identification of genes enriched in specific cells. *Nucleic Acids
1235 Res.* 2010;38: 4218–4230. doi:10.1093/nar/gkq130

1236 114. Miller JA, Ding S-L, Sunkin SM, Smith KA, Ng L, Szafer A, et al. Transcriptional
1237 landscape of the prenatal human brain. *Nature*. 2014;508: 199–206.
1238 doi:10.1038/nature13185

1239 115. Sive HL, Grainger RM, Harland RM. Microinjection of *Xenopus* Oocytes. *Cold
1240 Spring Harb Protoc.* 2010;2010: pdb.prot5536. doi:10.1101/pdb.prot5536

1241 116. Lowery LA, Faris AER, Stout A, Van Vactor D. Neural Explant Cultures from
1242 *Xenopus laevis*. *J Vis Exp.* 2012; e4232. doi:10.3791/4232

1243 117. Nieuwkoop PD, Faber J. Normal table of *Xenopus laevis* (Daudin) : a systematical and
1244 chronological survey of the development from the fertilized egg till the end of
1245 metamorphosis. New York : Garland Pub; 1994.

1246 118. Hagberg AA, Schult DA, Swart PJ. Exploring network structure, dynamics, and
1247 function using NetworkX. 7th Python in Science Conference (SciPy 2008). 2008. pp.
1248 11–15.

1249 119. Carbon S, Ireland A, Mungall CJ, Shu S, Marshall B, Lewis S, et al. AmiGO: Online
1250 access to ontology and annotation data. *Bioinformatics*. 2009;25: 288–289.
1251 doi:10.1093/bioinformatics/btn615

1252 120. Karimi K, Fortriede JD, Lotay VS, Burns KA, Wang DZ, Fisher ME, et al. Xenbase: A
1253 genomic, epigenomic and transcriptomic model organism database. *Nucleic Acids Res.*
1254 2018;46: D861–D868. doi:10.1093/nar/gkx936

1255 121. Greenwood S, Struhl G. Progression of the morphogenetic furrow in the *Drosophila*
1256 eye: The roles of Hedgehog, Decapentaplegic and the Raf pathway. *Development*.
1257 1999;126: 5795–5808.

1258 122. Thurmond J, Goodman JL, Strelets VB, Attrill H, Gramates LS, Marygold SJ, et al.
1259 FlyBase 2.0: The next generation. *Nucleic Acids Res.* 2019;47: D759–D765.
1260 doi:10.1093/nar/gky1003

1261 123. Bult CJ, Blake JA, Smith CL, Kadin JA, Richardson JE, Anagnostopoulos A, et al.

1262 Mouse Genome Database (MGD) 2019. *Nucleic Acids Res.* 2019;47: D801–D806.
1263 doi:10.1093/nar/gky1056

1264 124. Petrovski S, Wang Q, Heinzen EL, Allen AS, Goldstein DB. Genic Intolerance to
1265 Functional Variation and the Interpretation of Personal Genomes. *PLoS Genet.* 2013;9:
1266 e1003709. doi:10.1371/journal.pgen.1003709

1267 125. Lek M, Karczewski KJ, Minikel E V., Samocha KE, Banks E, Fennell T, et al.
1268 Analysis of protein-coding genetic variation in 60,706 humans. *Nature.* 2016;536:
1269 285–291. doi:10.1038/nature19057

1270 126. O’Leary NA, Wright MW, Brister JR, Ciufo S, Haddad D, McVeigh R, et al.
1271 Reference sequence (RefSeq) database at NCBI: Current status, taxonomic expansion,
1272 and functional annotation. *Nucleic Acids Res.* 2016;44: D733–D745.
1273 doi:10.1093/nar/gkv1189

1274 127. UniProt Consortium. UniProt: the universal protein knowledgebase. *Nucleic Acids
1275 Res.* 2018;46: 2699–2699. doi:10.1093/nar/gky092

1276 128. The Gene Ontology Consortium. The Gene Ontology Resource: 20 years and still
1277 GOing strong. *Nucleic Acids Res.* 2019;47: D330–D338. doi:10.1093/nar/gky1055

1278

1279 **FIGURE LEGENDS**

1280 **Fig. 1. Strategy for identifying cellular phenotypes and genetic interactions of homologs**
1281 **of 3q29 genes.**

1282 We first knocked down individual or pairs of 14 *Drosophila* homologs of human genes in the
1283 3q29 region using tissue-specific RNAi. After screening for global phenotypes of RNAi lines
1284 for individual homologs of 3q29 genes, we tested 314 pairwise gene interactions using the fly
1285 eye, and found that *Cbp20* (*NCBP2*) enhanced the phenotypes of other homologs of 3q29
1286 genes and also interacted with homologs of known neurodevelopmental genes outside of the
1287 3q29 region. Next, we assayed for deeper cellular and neuronal phenotypes of flies with
1288 individual and pairwise knockdown of homologs of 3q29 genes, and observed cellular defects
1289 due to disrupted apoptosis and cell cycle mechanisms. We confirmed our results by rescuing
1290 cellular phenotypes with overexpression of the apoptosis inhibitor *Diap1* and by analyzing
1291 genes differentially expressed with knockdown of homologs of 3q29 genes. Finally, we tested
1292 a subset of three homologs of 3q29 genes in the *X. laevis* vertebrate model system by
1293 injecting two- or four-cell stage embryos with GFP and morpholinos (MOs) for *X. laevis*
1294 homologs of 3q29 genes to observe abnormal eye morphology, as well as injecting one cell
1295 with GFP and MOs at the two-cell stage to observe abnormal brain morphology. We found
1296 similar developmental defects in *X. laevis* to those observed in *Drosophila*, including
1297 increased apoptosis that was enhanced with pairwise knockdown of homologs of 3q29 genes
1298 and rescued with overexpression of the apoptosis inhibitor *xiap*. *X. laevis* embryo diagrams
1299 were produced by Nieuwkoop and Faber [117] and provided by Xenbase [120].

1300
1301 **Fig. 2. Neurodevelopmental defects in flies with knockdown of individual homologs of**
1302 **3q29 genes.**

1303 (A) Percentage of flies with tissue-specific RNAi knockdown of homologs of 3q29 genes
1304 (listed with their human counterparts) that manifest lethality or developmental phenotypes.
1305 (B) Eight homologs of 3q29 genes with pan-neuronal RNAi knockdown showed defects in
1306 climbing ability over ten days (two-way repeated measures ANOVA, $p < 1 \times 10^{-4}$, $df = 8$,
1307 $F = 21.097$). Data represented show mean \pm standard deviation of 10 independent groups of
1308 10 flies for each homolog. (C) Representative brightfield adult eye images of flies with eye-
1309 specific *GMR-GAL4;UAS-Dicer2* (scale bar = 100 μ m) RNAi knockdown of individual
1310 homologs of 3q29 genes show rough eye phenotypes. The boxplot shows *Flynotyper*-derived
1311 phenotypic scores for eyes with knockdown of homologs of 3q29 genes ($n = 10-14$,
1312 $*p < 0.05$, one-tailed Mann-Whitney test with Benjamini-Hochberg correction). (D) Boxplot

1313 of adult eye area in flies with *GMR-GAL4* RNAi knockdown of fly homologs of 3q29 genes
1314 ($n = 13\text{--}16$, $^*p < 0.05$, two-tailed Mann–Whitney test with Benjamini–Hochberg correction).
1315 (E) Confocal images of pupal eyes (scale bar = 5 μm) stained with anti-DLG (top) and larval
1316 eye discs (scale bar = 30 μm) stained with anti-pH3 (middle) and anti-dcp1 (bottom) illustrate
1317 cellular defects posterior to the morphogenetic furrow (white box) upon knockdown of select
1318 fly homologs of 3q29 genes. Yellow circles in DLG images indicate cone cell defects, white
1319 circles indicate bristle cell defects, yellow arrows indicate rotation defects, and yellow
1320 arrowheads indicate secondary cell defects. We note that pupal eye images were taken at a
1321 higher intensity for lines with knockdown of *dlg1* to account for reduced expression of DLG
1322 (see Methods), as these images were only for visualization of cell boundaries in the pupal eye
1323 and not for any quantitative analysis. (F) Boxplot of pH3-positive cells in larval eye discs of
1324 flies with knockdown of homologs of 3q29 genes ($n = 9\text{--}12$, $^*p < 0.05$, two-tailed Mann–
1325 Whitney test with Benjamini–Hochberg correction). (G) Boxplot of dcp1-positive cells in
1326 larval eye discs of flies with knockdown of homologs of 3q29 genes ($n = 11\text{--}12$, $^*p < 0.05$,
1327 two-tailed Mann–Whitney test with Benjamini–Hochberg correction). All boxplots indicate
1328 median (center line), 25th and 75th percentiles (bounds of box), and minimum and maximum
1329 (whiskers), with red dotted lines representing the control median. Results for a subset of
1330 climbing ability, adult eye area, and pH3 staining experiments were replicated in independent
1331 experimental batches (S14 Fig.). A list of full genotypes for fly crosses used in these
1332 experiments is provided in S2 File.

1333

1334 **Fig. 3. Screening for pairwise interactions of fly homologs of 3q29 genes in the**
1335 ***Drosophila* eye and nervous system.**

1336 (A) Heatmap showing average changes in phenotypic scores for pairwise *GMR-GAL4* RNAi
1337 knockdown of fly homologs of 3q29 genes in the adult eye, compared with recombined lines
1338 for individual homologs of 3q29 genes crossed with controls. Gray boxes indicate crosses
1339 without available data. Boxplots of phenotypic scores for pairwise knockdown of (B) *Cbp20*
1340 and (C) *dlg1* with other fly homologs of 3q29 genes are shown ($n = 5\text{--}14$, $^*p < 0.05$, two-
1341 tailed Mann–Whitney test with Benjamini–Hochberg correction). Green arrows indicate an
1342 example pair of reciprocal lines showing enhanced phenotypes compared with their
1343 respective single-hit recombined controls. Crosses with the mutant line *Tsf2*^{KG01571} are
1344 included along with RNAi lines for other homologs of 3q29 genes, as eye-specific RNAi
1345 knockdown of *Tsf2* was lethal. (D) Representative brightfield adult eye images of flies with
1346 pairwise knockdown of fly homologs of 3q29 genes (scale bar = 100 μm) show enhancement

1347 (Enh.) of rough eye phenotypes compared with recombined lines for individual homologs of
1348 3q29 genes crossed with controls. **(E)** Representative confocal images of larval eye discs
1349 stained with anti-chaoptin (scale bar = 30 μ m) illustrate enhanced defects (Enh.) in axon
1350 targeting (white arrows) from the retina to the optic lobes of the brain with eye-specific
1351 knockdown of *Cbp20/dlg1* and *Cbp20/Fsn* compared with *Cbp20* knockdown. Note that n=9-
1352 17 larval eye disc preparations were assessed for each tested interaction. **(F)** Flies with pan-
1353 neuronal *Elav-GAL4* pairwise knockdown of homologs of 3q29 genes showed enhanced
1354 defects in climbing ability over ten days (two-way repeated measures ANOVA, $p < 4.00 \times 10^{-4}$,
1355 $df = 2$, $F = 7.966$) compared with recombined *Cbp20* knockdown crossed with control. Data
1356 represented show mean \pm standard deviation of 10 independent groups of 10 flies for each
1357 line tested. Results for the climbing assays were replicated in an independent experimental
1358 batch (**S14 Fig.**). All boxplots indicate median (center line), 25th and 75th percentiles
1359 (bounds of box), and minimum and maximum (whiskers), with red dotted lines representing
1360 the control median. A list of full genotypes for fly crosses used in these experiments is
1361 provided in **S2 File**.

1362

1363 **Fig. 4. Connectivity of 3q29 genes in human gene interaction databases.**

1364 **(A)** Genetic interactions of 3q29 genes in the context of a general human gene interaction
1365 network (GeneMania). The strongly connected component includes 11/21 total 3q29 genes.
1366 Black-shaded nodes represent the input 3q29 genes, while grey nodes represent connector
1367 genes in the network. Edge color represents the interaction data source (purple: co-
1368 expression, orange: predicted interaction), while edge thickness represents weighted scores
1369 for each interaction. **(B)** Genetic interactions of 19 genes in the 3q29 region in the context of
1370 a brain-specific human gene interaction network (GIANT). Large nodes represent the input
1371 3q29 genes, while small nodes represent connector genes in the network. Edge color
1372 represents the weighted score for each interaction, from low connectivity (green) to high
1373 connectivity (red). **(C)** Histograms and smoothed normal distributions showing the average
1374 connectivity among genes in the 3q29 region (blue) along with two other large CNVs,
1375 16p11.2 (red) and 22q11.2 deletion (green), within a brain-specific gene interaction network.
1376 Average connectivity is measured as the shortest weighted distance between two genes, with
1377 lower distances representing higher connectivity. Genes within the 3q29 and 22q11.2
1378 deletions were not significantly more connected to each other ($p > 0.05$, one-tailed Mann-
1379 Whitney test with Benjamini-Hochberg correction) than random sets of 21 genes throughout
1380 the genome (grey). However, genes within the 16p11.2 region were significantly more

1381 connected to each other than the random gene sets ($p=0.003$, one-tailed Mann-Whitney test
1382 with Benjamini-Hochberg correction). **(D)** Pairwise connectivity of individual 3q29 genes
1383 within a brain-specific gene interaction network, excluding six genes not present in the
1384 network (*RNF168*, *ZDHHC19*, *LRRC33*, *OSTalpha*, *SMCO1*, and *TCTEX1D2*). Average
1385 connectivity is measured as the shortest weighted distance between two genes, with lower
1386 values representing higher connectivity. Underlined genes have a higher average connectivity
1387 ($p<0.05$, one-tailed Mann-Whitney test with Benjamini-Hochberg correction) to other genes
1388 in the region compared with random sets of 21 genes throughout the genome.

1389

1390 **Fig. 5. Cellular phenotypes with pairwise knockdown of fly homologs of 3q29 genes.**
1391 **(A)** Representative brightfield adult eye images (scale bar = 100 μm) show that heterozygous
1392 *GMR-GAL4* RNAi knockdown of *dlg1* enhanced the rough eye phenotype and necrotic
1393 patches (yellow circles) of flies heterozygous or homozygous for *Cbp20* RNAi. **(B)**
1394 Representative confocal images of pupal eyes (scale bar = 5 μm) stained with anti-DLG
1395 illustrate enhanced defects in ommatidial organization upon concomitant knockdown of
1396 *Cbp20* with other fly homologs of 3q29 genes compared with *Cbp20* knockdown. Yellow
1397 circles in DLG images indicate cone cell defects, white circles indicate bristle cell defects,
1398 yellow arrows indicate rotation defects, and yellow arrowheads indicate secondary cell
1399 defects. We note that pupal eye images were taken at a higher intensity for lines with
1400 knockdown of *Cbp20/dlg1* to account for reduced expression of DLG (see Methods), as these
1401 images were only for visualization of cell boundaries in the pupal eye and not for any
1402 quantitative analysis. **(C)** Representative confocal images of pupal eyes (scale bar = 5 μm)
1403 stained with Phalloidin illustrate enhanced defects in photoreceptor cell count and
1404 organization upon concomitant knockdown of *Cbp20* and other fly homologs of 3q29 genes
1405 compared with *Cbp20* knockdown. **(D)** Representative confocal images of larval eye discs
1406 (scale bar = 30 μm) stained with anti-dcp1 (top) and anti-pH3 (bottom) show enhanced
1407 defects in apoptosis and cell proliferation with pairwise knockdown of *Cbp20* and other fly
1408 homologs of 3q29 genes compared with recombined *Cbp20* knockdown crossed with
1409 controls. **(E)** Boxplot of dcp1-positive cells in the larval eye discs of flies with pairwise
1410 knockdown of homologs of 3q29 genes ($n = 10-11$, $*p < 0.05$, two-tailed Mann-Whitney test
1411 with Benjamini-Hochberg correction). **(F)** Boxplot of pH3-positive cells in the larval eye
1412 discs of flies with pairwise knockdown of homologs of 3q29 genes ($n = 10-12$, $*p < 0.05$,
1413 two-tailed Mann-Whitney test with Benjamini-Hochberg correction). All boxplots indicate
1414 median (center line), 25th and 75th percentiles (bounds of box), and minimum and maximum

1415 (whiskers), with red dotted lines representing the control median. A list of full genotypes for
1416 fly crosses used in these experiments is provided in **S2 File**.

1417

1418 **Fig. 6. Rescue of cellular phenotypes due to knockdown of fly homologs of 3q29 genes**
1419 **with overexpression of the apoptosis inhibitor *Diap1*.**

1420 (A) Representative brightfield adult eye images (scale bar = 100 μ m) show rescue of rough
1421 eye phenotypes for flies with concomitant *GMR-GAL4* RNAi knockdown of *Cbp20* or *dlg1*
1422 and overexpression of *Diap1*, as well as enhanced (Enh.) phenotypes with overexpression of
1423 caspase-9 homolog *Dronc*. (B) Boxplot of phenotypic scores for flies with knockdown of
1424 *Cbp20* or *dlg1* and overexpression of *Diap1* or *Dronc* (n = 8–9, *p < 0.05, two-tailed Mann–
1425 Whitney test with Benjamini-Hochberg correction) is shown. (C) Box plot showing area of
1426 necrotic patches in adult fly eyes with knockdown of *Cbp20* and overexpression of *Dronc*
1427 (n=9, *p=1.14×10⁻⁴, one-tailed Mann–Whitney test with Benjamini-Hochberg correction) is
1428 shown. (D) Confocal images of pupal eyes (scale bar = 5 μ m) stained with anti-DLG illustrate
1429 the rescue of ommatidial organization defects due to knockdown of *Cbp20* or *dlg1* upon
1430 overexpression of *Diap1*. Yellow circles in DLG images indicate cone cell defects, white
1431 circles indicate bristle cell defects, yellow arrows indicate rotation defects, and yellow
1432 arrowheads indicate secondary cell defects. We note that pupal eye images were taken at a
1433 higher intensity for lines with knockdown of *dlg1* to account for reduced expression of DLG
1434 (see Methods), as these images were only for visualization of cell boundaries in the pupal eye
1435 and not for any quantitative analysis. (E) Larval eye discs (scale bar = 30 μ m) stained with
1436 anti-dcp1 show rescue of apoptosis phenotypes observed in flies with *Cbp20* and *dlg1*
1437 knockdown upon *Diap1* overexpression as well as enhanced (Enh.) phenotypes upon *Dronc*
1438 overexpression. (F) Boxplot of dcp1-positive cells in the larval eye discs of flies with
1439 knockdown of *Cbp20* or *dlg1* and *Diap1* or *Dronc* overexpression (n = 9–18, *p < 0.05, two-
1440 tailed Mann–Whitney test with Benjamini-Hochberg correction). (G) Representative confocal
1441 images of larval eye discs stained with anti-chaoptin (scale bar = 30 μ m) illustrate the
1442 suppression (Supp.) of axon targeting defects (white arrows) observed in flies due to
1443 knockdown of *Cbp20* or *dlg1* with overexpression of *Diap1*. Note that n=8-18 larval eye disc
1444 preparations were assessed for each interaction cross tested. All boxplots indicate median
1445 (center line), 25th and 75th percentiles (bounds of box), and minimum and maximum
1446 (whiskers), with red dotted lines representing the control median. A list of full genotypes for
1447 fly crosses used in these experiments is provided in **S2 File**.

1448

1449 **Fig. 7. Pairwise interactions between fly homologs of 3q29 genes and other**
1450 **neurodevelopmental genes.**

1451 (A) Heatmap showing the average changes in phenotypic scores for the *GMR-GAL4* pairwise
1452 RNAi knockdown of fly homologs for 3q29 genes and other neurodevelopmental genes
1453 (along with their human counterparts) in the adult eye, compared with recombined lines for
1454 individual homologs of 3q29 genes crossed with controls. (B) Representative brightfield adult
1455 eye images of flies with pairwise knockdown of fly homologs for 3q29 genes and known
1456 neurodevelopmental genes (scale bar = 100 μ m) show enhancement (Enh.) or suppression
1457 (Supp.) of rough eye phenotypes and necrotic patches compared with flies with knockdown
1458 of individual homologs of neurodevelopmental genes. A list of full genotypes for fly crosses
1459 used in these experiments is provided in **S2 File**.

1460

1461 **Fig. 8. Developmental phenotypes observed with knockdown of homologs of 3q29 genes**
1462 **in *X. laevis* models.**

1463 (A) To study brain morphology upon knockdown of *X. laevis* homologs of genes in the 3q29
1464 region, one cell in a two-cell embryo was injected with single or multiple MOs for homologs
1465 of 3q29 genes while the other cell remained uninjected. Representative images of stage 47 *X.*
1466 *laevis* tadpoles (scale bar = 500 μ m) with MO knockdown of *ncbp2*, *fbxo45* and *pak2* show
1467 morphological defects and decreased size, including decreased forebrain (highlighted in red
1468 on the control image) and midbrain (highlighted in yellow) area, compared with control
1469 tadpoles. Pairwise knockdown of *fbxo45* and *ncbp2* enhanced these phenotypes, which were
1470 also rescued with overexpression of *xiap*. (B) Box plot of forebrain area in *X. laevis* models
1471 with knockdown of homologs of 3q29 genes, normalized to controls ($n = 30$ –63, $^*p < 0.05$,
1472 two-tailed Welch's T-test with Benjamini-Hochberg correction). Red box indicates rescue of
1473 decreased *ncbp2* forebrain area with overexpression of the apoptosis inhibitor *xiap*. (C) Box
1474 plot of midbrain area in *X. laevis* models with knockdown of homologs of 3q29 genes,
1475 normalized to controls ($n = 30$ –63, $^*p < 0.05$, two-tailed Welch's T-test with Benjamini-
1476 Hochberg correction). Red box indicates rescue of decreased *ncbp2* midbrain area with
1477 overexpression of the apoptosis inhibitor *xiap*. (D) Western blot analysis of *X. laevis* whole
1478 embryos show increased intensity of cleaved caspase-3 bands at 19kD and 17kD with
1479 knockdown of homologs of 3q29 genes, including enhanced caspase-3 levels with
1480 knockdown of multiple homologs of 3q29 genes and rescued levels with *xiap* overexpression.
1481 β -actin was used as a loading control on the same blot. Representative western blot images
1482 shown are cropped; the full blots for both replicates are provided in **S12 Fig.** (E)

1483 Quantification of western blot band intensity for caspase-3 levels, normalized to the loading
1484 control. Red box indicates rescue of increased caspase-3 levels with overexpression of the
1485 apoptosis inhibitor *xiap*. All boxplots indicate median (center line), 25th and 75th percentiles
1486 (bounds of box), and minimum and maximum (whiskers), with red dotted lines representing
1487 the control median. The data shown for the brain area experiments represent pooled results of
1488 three experimental batches, and were normalized to the respective controls from each batch.
1489 *X. laevis* embryo diagrams were produced by Nieuwkoop and Farber [117] and provided by
1490 Xenbase [120].

1491

1492 **Fig. 9. Interactions between *NCBP2* and other homologs of 3q29 genes contribute to**
1493 **neurodevelopmental defects through conserved cellular pathways.**

1494 (A) We identified 44 interactions between pairs of *Drosophila* homologs of 3q29 genes. With
1495 the exception of *Ulp1* (*SENP5*), the cellular phenotypes of each homolog were significantly
1496 enhanced with simultaneous knockdown of *Cbp20*. While other homologs of 3q29 genes also
1497 interact with each other, our data suggest that *Cbp20* is a key modulator of cellular
1498 phenotypes within the deletion region. (B) Schematic representing the network context of
1499 *NCBP2* and other genes in the 3q29 region towards neurodevelopmental phenotypes. We
1500 propose that the effects of *NCBP2* disruption propagate through a network of functionally-
1501 related genes, including other 3q29 genes (highlighted in blue), leading to a cascade of
1502 disruptions in key biological mechanisms, including apoptosis and cell cycle pathways. These
1503 pathways jointly contribute towards the observed neurodevelopmental phenotypes.

1504

1505 **SUPPORTING INFORMATION LEGENDS**

1506 **S1 Fig. Developmental defects in flies with tissue-specific knockdown of individual**
1507 **homologs of 3q29 genes.**

1508 (A) Images of adult fly wings (scale bar = 500um) show a range of phenotypic defects due to
1509 wing-specific *bx^{MS1096}-GAL4* RNAi knockdown of fly homologs of 3q29 genes. (B) Adult
1510 flies with pan-neuronal RNAi knockdown of *dlg1* showed approximately 30% lethality
1511 between days 1-4 (one-way repeated measures ANOVA, $p < 1 \times 10^{-4}$, $df = 1$, $F = 54.230$), which
1512 was not observed in control *Elav-GAL4* or *Cbp20* knockdown flies. Data represented shows
1513 mean \pm standard deviation of 10 independent groups of 10 flies for each homolog. (C)
1514 Representative confocal images of larval eye discs stained with anti-chaoptin (scale
1515 bar = 30 μ m) illustrate defects in axon targeting (highlighted by white arrows) from the retina
1516 to the optic lobes of the brain upon eye-specific knockdown of fly homologs of 3q29 genes.
1517 Note that $n=8-20$ larval eye disc preparations were assessed for each RNAi line tested. A list
1518 of full genotypes for fly crosses used in these experiments is provided in **S2 File**.

1519

1520 **S2 Fig. Examination of cellular phenotypes in the *Drosophila* eye.**

1521 We tested individual and pairwise knockdown of fly homologs of 3q29 genes for cellular
1522 phenotypes in the adult, pupal and larval eyes. (A) We first used the *Flynotyper* software [53]
1523 to quantify the degree of ommatidial disorganization leading to rough eye phenotypes in adult
1524 flies, as represented by the distance and angles between adjacent ommatidia (yellow arrows).
1525 (B) We next stained pupal eyes with anti-DLG to observe changes in the number and
1526 arrangement of ommatidial cells, including cone cells (c), bristle cells (b), and primary,
1527 secondary and tertiary cells (1,2,3). We also examined the organization of the photoreceptor
1528 cells (R1-R7, with R8 not visible) in each ommatidium by staining the pupal eyes with
1529 Phalloidin. (C) We finally stained larval eye discs with markers for cellular processes, such
1530 as pH3 for proliferating cells and dcp1 for apoptosis. As the progression of the
1531 morphogenetic furrow (MF) across the larval eye discs leads to proliferation and
1532 differentiation of photoreceptor neurons [121], we examined changes in the number of
1533 stained cells posterior to the MF. (D) Scatter plot of dcp1, pH3, TUNEL, and BrdU-positive
1534 cell counts in larval eye discs with knockdown of homologs of 3q29 genes quantified using
1535 two ImageJ plugins, AnalyzeParticles and Image-based Tool for Counting Nuclei (ITCN). As
1536 the two methods showed a strong correlation with each other (Pearson correlation, $n=285$,
1537 $r=0.736$, $p < 2.2 \times 10^{-16}$), we used ITCN counts to display cell count data in the manuscript.

1538

1539 **S3 Fig. Phenotypic screening for flies with eye-specific knockdown of individual fly**
1540 **homologs of 3q29 genes.**

1541 (A) Representative brightfield adult eye images of flies with *GMR-GAL4;UAS-Dicer2* RNAi
1542 knockdown of fly homologs of 3q29 genes (scale bar = 100 μ m) show a wide range of
1543 phenotypic severity. (B) Box plot of average ommatidial diameter in flies with *GMR-GAL4*
1544 knockdown of select fly homologs of 3q29 genes is shown (n = 15, *p < 0.05, two-tailed
1545 Mann–Whitney test with Benjamini-Hochberg correction). (C) Box plot of phenotypic scores
1546 derived from *Flynotyper* for eye-specific *dCad-GFP*, *GMR-GAL4* RNAi knockdown of 13 fly
1547 homologs of 3q29 genes is shown (n = 5–20, *p < 0.05, one-tailed Mann–Whitney test with
1548 Benjamini-Hochberg correction). (D) Box plot of phenotypic scores derived from *Flynotyper*
1549 for eye-specific *GMR-GAL4;UAS-Dicer2* (left) and *dCad-GFP*, *GMR-GAL4* (right) RNAi
1550 knockdown of nine validation lines for fly homologs of 3q29 genes is shown (n = 5–14,
1551 *p < 0.05, one-tailed Mann–Whitney test with Benjamini-Hochberg correction). All boxplots
1552 indicate median (center line), 25th and 75th percentiles (bounds of box), and minimum and
1553 maximum (whiskers), with red dotted lines representing the control median. A list of full
1554 genotypes for fly crosses used in these experiments is provided in **S2 File**.

1555

1556 **S4 Fig. Cellular phenotypes of flies with eye-specific knockdown of individual fly**
1557 **homologs of 3q29 genes.**

1558 (A) Confocal images of pupal eyes (scale bar = 5 μ m) stained with anti-DLG illustrate a range
1559 of defects in ommatidial organization upon *GMR-GAL4* RNAi knockdown of fly homologs
1560 of 3q29 genes. Yellow circles indicate cone cell defects, white circles indicate bristle cell
1561 defects, yellow arrows indicate rotation defects, and yellow arrowheads indicate secondary
1562 cell defects. (B) Confocal images of pupal eyes (scale bar = 5 μ m) stained with Phalloidin
1563 illustrate defects in photoreceptor cell count and organization upon knockdown of fly
1564 homologs of 3q29 genes. (C) Confocal images of larval eye discs (scale bar = 30 μ m) stained
1565 with anti-pH3 illustrate changes in cell proliferation upon knockdown of select fly homologs
1566 of 3q29 genes. (D) Larval eye discs (scale bar = 30 μ m) stained with BrdU (top) and TUNEL
1567 (bottom) illustrate abnormal cell cycle and apoptosis defects, respectively, due to eye-specific
1568 knockdown of *Cbp20* and *dlg1*. (E) Box plot of BrdU-positive cells in the larval eye discs of
1569 flies with knockdown of *dlg1* and *Cbp20* is shown (n = 7–12, *p < 0.05, two-tailed Mann–
1570 Whitney test with Benjamini-Hochberg correction). (F) Box plot of TUNEL-positive cells in
1571 the larval eye discs of flies with knockdown of *dlg1* and *Cbp20* is shown (n = 8, *p < 0.05,
1572 two-tailed Mann–Whitney test with Benjamini-Hochberg correction). Results for the TUNEL

1573 staining experiments were replicated in an independent experimental batch (**S14 Fig.**). All
1574 boxplots indicate median (center line), 25th and 75th percentiles (bounds of box), and
1575 minimum and maximum (whiskers), with red dotted lines representing the control median. A
1576 list of full genotypes for fly crosses used in these experiments is provided in **S2 File**.

1577

1578 **S5 Fig. Cellular phenotypes of flies with wing-specific knockdown of individual fly**
1579 **homologs of 3q29 genes.**

1580 (A) Larval wing discs (scale bar = 50 μ m) stained with pH3 illustrate abnormal cell
1581 proliferation due to RNAi knockdown of select fly homologs of 3q29 genes, compared with
1582 appropriate VDRC GD and KK bx^{MS1096} -*GAL4* controls. We examined changes in the number
1583 of stained cells within the wing pouch of the wing disc (white box), which becomes the adult
1584 wing. (B) Box plot of pH3-positive cells in the larval wing discs of flies with knockdown of
1585 select fly homologs of 3q29 genes is shown ($n = 8–15$, $*p < 0.05$, two-tailed Mann–Whitney
1586 test with Benjamini–Hochberg correction). (C) Larval wing discs (scale bar = 50 μ m) stained
1587 with anti-dcp1 show abnormal apoptosis due to knockdown of select fly homologs of 3q29
1588 genes compared with appropriate VDRC GD and KK bx^{MS1096} -*GAL4* controls. (D) Box plot
1589 of dcp1-positive cells in the larval wing discs of flies with knockdown of select fly homologs
1590 of 3q29 genes is shown ($n = 8–15$, $*p < 0.05$, two-tailed Mann–Whitney test with Benjamini–
1591 Hochberg correction). *Cbp20* flies showed severe dcp1 staining across the entire wing pouch
1592 and could not be quantified. All boxplots indicate median (center line), 25th and 75th
1593 percentiles (bounds of box), and minimum and maximum (whiskers), with red dotted lines
1594 representing the control median. A list of full genotypes for fly crosses used in these
1595 experiments is provided in **S2 File**.

1596

1597 **S6 Fig. Phenotypic screening for pairwise interactions of homologs of 3q29 genes in the**
1598 **adult fly eye.**

1599 (A) Heatmap showing average changes in phenotypic scores for pairwise *GMR-GAL4* RNAi
1600 knockdown of fly homologs of 3q29 genes in the adult eye, compared with recombined lines
1601 for individual homologs of 3q29 genes crossed with controls, is shown. Gray boxes indicate
1602 crosses without available data. Crosses with the mutant line *Tsf2*^{KG01571} are also included
1603 along with RNAi lines for other homologs of 3q29 genes, as eye-specific RNAi knockdown
1604 of *Tsf2* was lethal. (B–H) Box plots of phenotypic scores for pairwise knockdowns of
1605 homologs of 3q29 genes compared with recombined lines for individual homologs of 3q29
1606 genes crossed with controls are shown ($n = 5–12$, $*p < 0.05$, two-tailed Mann–Whitney test

1607 with Benjamini-Hochberg correction). All boxplots indicate median (center line), 25th and
1608 75th percentiles (bounds of box), and minimum and maximum (whiskers), with red dotted
1609 lines representing the control median. A list of full genotypes for fly crosses used in these
1610 experiments is provided in **S2 File**.

1611

1612 **S7 Fig. Validation lines for pairwise interactions of homologs of 3q29 genes in the adult**
1613 **fly eye.**

1614 (A-F) Box plots of phenotypic scores for pairwise *GMR-GAL4* RNAi knockdown of select
1615 fly homologs of 3q29 genes (*Cbp20*, *CG8888*, *dlg1*, *Fsn*, *Pak*, and *PIG-Z*) with validation
1616 RNAi and mutant lines for other homologs of 3q29 genes, compared with recombined lines
1617 for individual homologs of 3q29 genes crossed with controls, are shown (n = 4–14, *p < 0.05,
1618 two-tailed Mann–Whitney test with Benjamini-Hochberg correction), are shown. These
1619 crosses include flies homozygous for *Cbp20* RNAi as well as flies homozygous for *Cbp20*
1620 RNAi and heterozygous for *dlg1* RNAi (green arrows). Note that the phenotypic scores
1621 derived from *Flynotyper* may not accurately capture the necrotic patches observed in these
1622 crosses. All boxplots indicate median (center line), 25th and 75th percentiles (bounds of box),
1623 and minimum and maximum (whiskers), with red dotted lines representing the control
1624 median. A list of full genotypes for fly crosses used in these experiments is provided in **S2**
1625 **File**.

1626

1627 **S8 Fig. Transcriptome analysis of flies with knockdown of select homologs of 3q29**
1628 **genes.**

1629 (A) Clusters of Gene Ontology terms enriched among differentially-expressed fly genes
1630 (blue) and their corresponding human homologs (red) with individual and pairwise *Elav-*
1631 *GAL4* RNAi knockdown of fly homologs of 3q29 genes (p < 0.05, Fisher's Exact test with
1632 Benjamini-Hochberg correction) are shown. Black boxes indicate enrichment of each gene
1633 set for clusters of Gene Ontology terms. Full lists of enriched GO terms are provided in **S3**
1634 **File**. (B) Enrichments for shared and unique differentially-expressed fly genes (blue) and
1635 their corresponding human homologs (red) with individual knockdown of *Cbp20* and *Fsn*, as
1636 well as concomitant knockdown of *Cbp20/Fsn*, are shown. We found 229 genes uniquely
1637 dysregulated in flies with pairwise knockdown of *Fsn* and *Cbp20*, which were enriched for
1638 cell cycle function (p = 0.011 for fly gene enrichment and p = 1.12 × 10⁻⁸ for human homologs,
1639 Fisher's Exact test with Benjamini-Hochberg correction). (C) Diagram showing human cell
1640 cycle and apoptosis genes whose fly homologs are differentially expressed with knockdown

1641 of *Cbp20* and *Fsn*, as well as concomitant knockdown of *Cbp20/Fsn*. Red boxes indicate
1642 apoptosis genes, green boxes indicate cell cycle genes, and yellow boxes indicate genes
1643 associated with both functions. **(D)** Enrichments of human homologs of genes differentially
1644 expressed in flies with knockdown of *Cbp20/Fsn* across different brain tissues and
1645 developmental timepoints are shown (Specific Expression Analysis). The size of each
1646 hexagon represents the number of genes preferentially expressed at each tissue and timepoint,
1647 with concentric hexagons representing bins of genes with stronger levels of preferential
1648 expression. The shading of each hexagon represents the enrichment of differentially-
1649 expressed genes among genes preferentially expressed at each timepoint ($p < 0.1$, Fisher's
1650 Exact test with Benjamini-Hochberg correction). A list of full genotypes for fly crosses used
1651 in these experiments is provided in **S2 File**.

1652

1653 **S9 Fig. Cellular phenotypes for pairwise knockdowns of homologs of 3q29 genes.**
1654 **(A)** Box plot showing the area of necrotic patches in adult fly eyes with pairwise knockdown
1655 of homologs of 3q29 genes ($n=5-13$, $*p < 0.05$, one-tailed Mann-Whitney test with
1656 Benjamini-Hochberg correction). Flies with knockdown of *Cbp20* and *Fsn*, *dlg1* and *arm*
1657 showed enhanced necrotic patches compared with knockdown of *Cbp20*, while homozygous
1658 *Cbp20* RNAi and concomitant knockdown of *dlg1* showed increased necrotic patches
1659 compared with homozygous *Cbp20* RNAi. Furthermore, flies with knockdown of *dlg1* and
1660 *arm* both showed enhanced necrotic patches compared with individual knockdown of *dlg1* or
1661 *arm*. **(B)** Confocal images of pupal eyes (scale bar = 5 μ m) stained with anti-DLG (top) and
1662 Phalloidin (bottom) illustrate enhanced defects in ommatidial and photoreceptor cell
1663 organization with concomitant *GMR-GAL4* RNAi knockdown of *Cbp20* and other fly
1664 homologs of 3q29 genes compared with *Cbp20* knockdown. **(C)** Larval eye discs (scale
1665 bar = 30 μ m) stained with TUNEL show increases in apoptosis with pairwise knockdown of
1666 *Cbp20* and other fly homologs of 3q29 genes compared with recombined *Cbp20* knockdown
1667 crossed with control. **(D)** Box plot of TUNEL-positive cells in the larval eye discs of flies
1668 with pairwise knockdown of homologs of 3q29 genes ($n = 9-13$, $*p < 0.05$, two-tailed Mann-
1669 Whitney test with Benjamini-Hochberg correction). All boxplots indicate median (center
1670 line), 25th and 75th percentiles (bounds of box), and minimum and maximum (whiskers),
1671 with red dotted lines representing the control median. A list of full genotypes for fly crosses
1672 used in these experiments is provided in **S2 File**.

1673

1674

1675 **S10 Fig. Rescue of cellular phenotypes due to knockdown of fly homologs of 3q29 genes**
1676 **with overexpression of *Diap1*.**

1677 (A) Cellular phenotypes of flies with overexpression of *Diap1* and *Dronc*. Representative
1678 brightfield adult eye images (scale bar = 100 μ m) and confocal images of larval eye discs
1679 (scale bar = 30 μ m) stained with anti-dcp1 are shown for flies with *GMR-GAL4*
1680 overexpression of *Diap1* and *Dronc*, while confocal images of pupal eyes (scale bar = 5 μ m)
1681 stained with anti-DLG are also shown for flies with overexpression of *Diap1*. While the
1682 overexpression of *Diap1* did not lead to any changes in the pupal or adult eye phenotype,
1683 overexpression of *Dronc* resulted in a large increase in apoptosis and depigmentation in the
1684 adult eye. (B) Box plot of *Flynotyper* distance ommatidial disorderliness (OD) scores for flies
1685 with concomitant *GMR-GAL4* RNAi knockdown of *Cbp20* or *dlg1* and overexpression of
1686 *Diap1* or *Dronc* is shown (n = 8–9, *p < 0.05, two-tailed Mann–Whitney test with Benjamini–
1687 Hochberg correction). (C) Box plot of *Flynotyper* angle OD scores for flies with knockdown
1688 of *Cbp20* or *dlg1* and overexpression of *Diap1* or *Dronc* is shown (n = 8–9, *p < 0.05, two-
1689 tailed Mann–Whitney test with Benjamini–Hochberg correction). The distance and angle OD
1690 scores, component subscores derived from *Flynotyper* [53], mirror the trends observed in the
1691 overall phenotypic scores (Figure 6B). (D) Box plot of adult eye area in flies with
1692 knockdown of *Cbp20* or *dlg1* and overexpression of *Diap1* or *Dronc* is shown (n = 8–9,
1693 *p < 0.05, two-tailed Mann–Whitney test with Benjamini–Hochberg correction). (E) Confocal
1694 images of pupal eyes (scale bar = 5 μ m) stained with Phalloidin illustrate the rescue of
1695 photoreceptor cell organization defects due to knockdown of *Cbp20* or *dlg1* upon
1696 overexpression of *Diap1*. (F) Larval eye discs (scale bar = 30 μ m) stained with TUNEL show
1697 rescue of apoptosis phenotypes observed in flies with knockdown of *Cbp20* or *dlg1* and
1698 overexpression of *Diap1*, as well as enhanced apoptosis with overexpression of *Dronc*. (G)
1699 Box plot of TUNEL-positive cells in the larval eye discs of flies with knockdown of *Cbp20*
1700 or *dlg1* and overexpression of *Diap1* or *Dronc* is shown (n = 7–10, *p < 0.05, two-tailed
1701 Mann–Whitney test with Benjamini–Hochberg correction). All boxplots indicate median
1702 (center line), 25th and 75th percentiles (bounds of box), and minimum and maximum
1703 (whiskers), with red dotted lines representing the control median. A list of full genotypes for
1704 fly crosses used in these experiments is provided in S2 File.

1705

1706 **S11 Fig. Phenotypic scores for interactions between homologs of 3q29 genes and known**
1707 **neurodevelopmental genes in the adult fly eye.**

1708 (A–D) Box plots of phenotypic scores for concomitant *GMR-GAL4* RNAi knockdown of fly

1709 homologs of 3q29 genes and neurodevelopmental genes, compared with recombined lines for
1710 individual homologs of 3q29 genes crossed with controls, are shown ($n = 2-10$, $*p < 0.05$,
1711 two-tailed Mann-Whitney test with Benjamini-Hochberg correction). All boxplots indicate
1712 median (center line), 25th and 75th percentiles (bounds of box), and minimum and maximum
1713 (whiskers), with red dotted lines representing the control median. A list of full genotypes for
1714 fly crosses used in these experiments is provided in **S2 File**.

1715

1716 **S12 Fig. Quantification of 3q29 morpholino knockdown and apoptosis marker levels in**
1717 ***X. laevis* models.**

1718 (A) Electrophoretic gels show decreased expression of homologs of 3q29 genes due to
1719 morpholino (MO) knockdown at various concentrations in *X. laevis* embryos. Three
1720 replicates (uninjected and two MO concentrations) were performed for each morpholino, and
1721 band intensities were compared with expression of *ODC1* controls taken from the same
1722 cDNA samples and run on gels processed in parallel. (B) Quantification of expression for
1723 homologs of 3q29 genes at different MO concentrations, as measured by band intensity ratio
1724 to *ODC1* controls ($n=3$ replicates, $*p < 0.05$, two-tailed Welch's T-test with Benjamini-
1725 Hochberg correction). (C) Full images of western blots for quantification of cleaved caspase-
1726 3 levels in *X. laevis* embryos with MO knockdown of homologs of 3q29 genes. Two replicate
1727 experiments were performed, and the intensity of bands at 19kD and 17kD (green arrows),
1728 corresponding with cleaved caspase-3, were normalized to those for the β -actin loading
1729 controls. Embryos injected with control MO, uninjected embryos, and embryos treated with
1730 30% EtOH as a positive control were included with the embryos injected with 3q29 MOs.

1731

1732 **S13 Fig. Eye phenotypes observed with knockdown of homologs of 3q29 genes in *X.***
1733 ***laevis* models.**

1734 (A) Representative eye images of stage 42 *X. laevis* tadpoles with MO knockdown of
1735 homologs of 3q29 genes (scale bar = 500 μ m) show defects in eye size and morphology
1736 compared with the control (top). These defects were rescued with co-injection and
1737 overexpression of mRNA for homologs of 3q29 genes, as well as overexpression of the
1738 apoptosis inhibitor *xiap* for *ncbp2* (bottom). (B) Box plot of eye area in *X. laevis* models with
1739 knockdown of homologs of 3q29 genes, normalized to controls, is shown ($n = 48-71$,
1740 $*p < 0.05$, two-tailed Welch's T-test with Benjamini-Hochberg correction). Models with
1741 *ncbp2* knockdown and *xiap* overexpression showed an increased eye size compared with
1742 *ncbp2* knockdown. (C) Box plot of eye area in *X. laevis* models with knockdown of

1743 homologs of 3q29 genes and overexpression of mRNA for homologs of 3q29 genes,
1744 normalized to controls, is shown ($n = 56\text{--}63$, $^*\text{p} < 0.05$, two-tailed Welch's T-test with
1745 Benjamini-Hochberg correction). All boxplots indicate median (center line), 25th and 75th
1746 percentiles (bounds of box), and minimum and maximum (whiskers), with red dotted lines
1747 representing the control median. The data shown for the eye area experiments represent
1748 pooled results of three experimental batches, and were normalized to the respective controls
1749 from each batch.

1750

1751 **S14 Fig. Replication of *Drosophila* experimental results for individual and pairwise**
1752 **knockdown of homologs of 3q29 genes.**

1753 (A) Replication dataset for climbing ability of select homologs of 3q29 genes over ten days.
1754 We replicated the defects in climbing ability observed with pan-neuronal RNAi knockdown
1755 of *Cbp20* and *dlg1*, while climbing defects in flies with knockdown of *Fsn* flies were not
1756 replicated in the second experimental batch and were therefore excluded from the main
1757 dataset (**Fig. 2B**). Data represented show mean \pm standard deviation of 7-10 independent
1758 groups of 10 flies for each homolog. (B) Replication dataset for climbing ability of pairwise
1759 knockdown of homologs of 3q29 genes over ten days. We replicated the defects in climbing
1760 ability observed with pan-neuronal RNAi knockdown of *Cbp20/dlg1* and *Cbp20/Fsn*
1761 compared with recombined *Cbp20* knockdown crossed with control (**Fig. 3F**). Data
1762 represented show mean \pm standard deviation of 5 independent groups of 10 flies for each
1763 homolog. (C) Replication dataset for adult eye area in flies with *GMR-GAL4* RNAi
1764 knockdown of homologs of 3q29 genes ($n = 10\text{--}14$, $^*\text{p} < 0.05$, two-tailed Mann-Whitney test
1765 with Benjamini-Hochberg correction). We replicated the decreased eye sizes in flies with
1766 knockdown of *Cbp20* and *CG8888*, while flies with knockdown of *dlg1* showed a non-
1767 significant ($p=0.154$) increase in eye size (**Fig. 2D**). (D) Confocal images for replication
1768 dataset larval eye discs (scale bar = 30 μm) stained with anti-pH3 (top) and TUNEL (bottom)
1769 illustrate cellular defects posterior to the morphogenetic furrow (white box) upon knockdown
1770 of select fly homologs of 3q29 genes (**Fig. 2E**). (E) Replication dataset for pH3-positive cells
1771 in larval eye discs of flies with knockdown of homologs of 3q29 genes ($n = 9\text{--}10$, two-tailed
1772 Mann-Whitney test with Benjamini-Hochberg correction). As in the main dataset (**Fig. 2F**),
1773 we observed no significant changes in cell proliferation for flies with knockdown of *Cbp20*
1774 and *dlg1*. (F) Replication dataset for TUNEL-positive cells in larval eye discs of flies with
1775 knockdown of homologs of 3q29 genes ($n = 6\text{--}8$, $^*\text{p} < 0.05$, two-tailed Mann-Whitney test
1776 with Benjamini-Hochberg correction). We replicated the increased apoptosis phenotypes

1777 observed with knockdown of *Cbp20* and *dlg1* (**S4 Fig.**). All boxplots indicate median (center
1778 line), 25th and 75th percentiles (bounds of box), and minimum and maximum (whiskers),
1779 with red dotted lines representing the control median. A list of full genotypes for fly crosses
1780 used in these experiments is provided in **S2 File**.

1781

1782 **S1 Table. *Drosophila* homologs of human 3q29 genes and expression of *Drosophila*
1783 homologs during development.**

1784 DIOPT version 7.1 [100] and reciprocal BLAST were used to identify fly homologs of genes
1785 within the 3q29 region; six genes did not have fly homologs. Expression levels of fly
1786 homologs of 3q29 genes were assessed using high-throughput expression data from FlyAtlas
1787 Anatomy microarray expression data [104] and modENCODE Anatomy RNA-Seq data [105]
1788 from FlyBase.

1789

1790 **S2 Table. qPCR primers and expression values for RNAi knockdown of fly homologs of
1791 3q29 genes.**

1792 *Elav-GAL4* flies were crossed with RNAi lines of fly homologs of 3q29 genes at 25°C, and 3-
1793 4 day old adult *Drosophila* heads were used to quantify the level of expression compared
1794 with *Elav-GAL4* controls. *Elav-GAL4*; *UAS-Dicer2* flies crossed with *CG5359* flies showed
1795 overexpression of *tiptop* [103] and were therefore excluded from further experiments. A list
1796 of full genotypes for fly crosses used in these experiments is provided in **S2 File**, and
1797 statistics for these data are provided in **S5 File**.

1798

1799 **S3 Table. Comparison of animal model phenotypes with knockdown or knockout of
1800 homologs of 3q29 genes.**

1801 Blue shaded boxes indicate previously identified phenotypes for individual homologs of 3q29
1802 genes, while “X” marks indicate recapitulated and novel phenotypes identified in our study.
1803 Gray-shaded boxes indicate that a homolog was not present in the model organism. Fly
1804 phenotypes were obtained from FlyBase [122], *X. laevis* phenotypes were obtained from
1805 Xenbase [120], and mouse knockout model phenotypes were obtained from the Mouse
1806 Genome Informatics database [123].

1807

1808 **S4 Table. Summary of scoring for phenotypic severity of axon targeting defects upon
1809 individual and pairwise knockdown of homologs of 3q29 genes.**

1810 Individual larval eye disc images were assigned mild, moderate or severe scores based on the

1811 severity of axon projection loss observed in each eye disc (see Methods). We found that the
1812 mild to moderate defects observed with knockdown of *Cbp20* were enhanced with
1813 concomitant knockdown of *dlg1* or *Fsn*, while *Diap1* overexpression partially rescued the
1814 defects observed with knockdown of *Cbp20* or *dlg1*. A list of full genotypes for fly crosses
1815 used in these experiments is provided in **S2 File**.

1816

1817 **S5 Table. Comparison of eye phenotypic scores for homologs of 3q29 genes and**
1818 **neurodevelopmental genes.**

1819 Table comparing *Flynotyper* scores for flies with *GMR-GAL4;UAS-Dicer2* RNAi knockdown
1820 of homologs of 3q29 genes (shaded in grey) with previously published scores for flies with
1821 *GMR-GAL4;UAS-Dicer2* RNAi knockdown of homologs of candidate neurodevelopmental
1822 genes [53].

1823

1824 **S6 Table. Analysis of defects in ommatidial cells with *GMR-GAL4* RNAi knockdown of**
1825 **fly homologs of 3q29 genes.**

1826 The number of “+” symbols displayed in the table indicate the severity of the observed
1827 cellular defects. Note that n=4-16 pupal eye preparations were assessed for each RNAi line
1828 tested. A list of full genotypes for fly crosses used in these experiments is provided in **S2**
1829 **File.**

1830

1831 **S7 Table. Screening for pairwise interactions among fly homologs of 3q29 genes.**

1832 “All interactions” indicates the number of pairwise crosses where at least one second-hit
1833 RNAi or mutant line showed enhancement of the single-hit phenotype, while “Validated”
1834 indicates the number of interactions which have two or more crosses with a second-hit RNAi
1835 or mutant line (if available) showing the same result. “Reciprocal cross” indicates the number
1836 of interactions with concordant results across pairs of reciprocal cross (i.e. *Cbp20/dlg1* vs.
1837 *dlg1/Cbp20*). These totals include crosses with the mutant line *Tsf2*^{KG01571}, as eye-specific
1838 RNAi knockdown of *Tsf2* was lethal, as well as flies heterozygous for *dlg1* RNAi and
1839 homozygous for *Cbp20* RNAi. Crosses with other RNAi or mutant lines for the same
1840 homolog (shaded in grey) are included as validation lines tested but were not counted as
1841 interactions. A list of full genotypes for fly crosses used in these experiments is provided in
1842 **S2 File.**

1843

1844 **S8 Table. Analysis of defects in ommatidial cells with pairwise *GMR-GAL4* RNAi**
1845 **knockdown of fly homologs of 3q29 genes.**

1846 The number of “+” symbols displayed in the table indicate the severity of the observed
1847 cellular defects. Note that n=4-16 pupal eye preparations were assessed for each interaction
1848 cross tested. A list of full genotypes for fly crosses used in these experiments is provided in
1849 **S2 File.**

1850

1851 **S9 Table. Screening for interactions between fly homologs of 3q29 genes and other**
1852 **known neurodevelopmental genes.**

1853 “All interactions” indicates the number of crosses where at least one second-hit RNAi line
1854 showed enhancement of the single-hit phenotype, while “Validated interactions” indicates the
1855 number of interactions which have two or more crosses with a second-hit RNAi or mutant
1856 line (if available) showing the same result. Results from two distinct fly homologs of
1857 *CHRNA7* that were crossed with homologs of 3q29 genes, *nAChRa6* and *nAChRa7*, were
1858 combined for the final number of interactions. Shaded interactions indicate pairwise crosses
1859 where the phenotypes observed with knockdown of the homolog for the neurodevelopmental
1860 gene by itself were suppressed with concomitant knockdown of homologs for 3q29 genes.
1861 The neurodevelopmental genes are annotated for cell cycle/apoptosis function (Gene
1862 Ontology terms GO:0007049 and GO:0006915) and association with microcephaly disorders
1863 [65]. A list of full genotypes for fly crosses used in these experiments is provided in **S2 File**.

1864

1865 **S10 Table. Developmental phenotypes observed in mouse models of the 3q29 deletion**
1866 **and individual homologs of 3q29 genes.**

1867 Comparison of mice with heterozygous deletion of the syntenic 3q29 region [14,15] with
1868 heterozygous knockout mouse models for *Dlg1* [14] and *Pak2* [72]. Blue shaded boxes
1869 indicate phenotypes observed in the knockout models, while gray-shaded boxes indicate a
1870 phenotype that was not tested in the knockout model. Neither *Dlg1*^{+/−} nor *Pak2*^{+/−} knockout
1871 mice recapitulate the body and brain weight, spatial learning and memory, or acoustic startle
1872 defects observed in the deletion mouse models.

1873

1874 **S11 Table. Summary of apoptosis function enrichment among candidate**
1875 **neurodevelopmental genes.**

1876 This table shows the number of candidate autism, intellectual disability and schizophrenia
1877 genes annotated for apoptosis function. The minimum, mean and maximum numbers of

1878 apoptosis genes in 100,000 simulated sets of candidate genes are shown, along with the
1879 percentiles and empirical p-values of the observed overlap with apoptosis genes for each
1880 simulation.

1881

1882 **S12 Table. Morpholinos used for *X. laevis* experiments.**

1883

1884 **S13 Table. qPCR primers used for *X. laevis* experiments.**

1885

1886 **S1 File. Pathogenicity metrics, mutations in disease cohorts, and biological functions of
1887 3q29 genes.**

1888 3q29 genes with Residual Variation Intolerance Scores (RVIS) <20th percentile [124] or
1889 probability of Loss-of-function Intolerant (pLI) scores >0.9 [125] are considered to be
1890 potentially pathogenic in humans and are shaded in gray. Mutations within 3q29 genes
1891 identified in disease cohorts were curated from three databases: denovo-db v.1.6.1 [75],
1892 GeneBook database (<http://atgu.mgh.harvard.edu/~spurcell/genebook/genebook.cgi>), and SFARI Gene [77]. Molecular functions for 3q29 genes were derived from
1893 RefSeq, UniProtKB and Gene Ontology (GO) individual gene summaries [126–128], and
1894 GO-SLIM terms for human genes and fly homologs were curated from PantherDB [101].
1895 Annotations for cell cycle/apoptosis and neuronal function were derived from GO Biological
1896 Process annotations for each gene.

1897

1898 **S2 File. List of fly stocks and full genotypes for all crosses tested.**

1900 This file lists the stock lines, stock center, and genotypes for primary and validation lines for
1901 fly homologs of 3q29 genes as well as neurodevelopmental and apoptosis genes outside of
1902 the 3q29 region. Full genotypes for the generated recombined lines as well as all individual
1903 and pairwise crosses tested in the manuscript are also listed in the file. BDSC: Bloomington
1904 *Drosophila* Stock Center; VDRC: Vienna *Drosophila* Resource Centre.

1905

1906 **S3 File. Transcriptome analysis of flies with knockdown of homologs of 3q29 genes.**

1907 This file lists all differentially expressed genes from RNA sequencing of flies with *Elav-*
1908 *GAL4* RNAi knockdown of homologs of 3q29 genes, as defined by log-fold change >1 or < -
1909 1 and false discovery rate (FDR) <0.05 (Benjamini-Hochberg correction). Human homologs
1910 identified using DIOPT are included for each differentially-expressed fly gene. The file also
1911 includes enriched Gene Ontology (GO) terms (p<0.05, Fisher's Exact test with Benjamini-

1912 Hochberg correction) for each set of differentially-expressed fly genes, as well as lists of GO
1913 terms enriched among their corresponding human homologs.

1914

1915 **S4 File. List of candidate neurodevelopmental genes with apoptosis function.**

1916 This file lists 525 candidate neurodevelopmental genes that are annotated for apoptosis GO
1917 terms, including their membership within pathogenic CNV regions.

1918

1919 **S5 File. Statistical analysis of experimental data.**

1920 This file shows all statistical information (sample size, mean/median/standard deviation of
1921 datasets, Shapiro-Wilk test statistics for normality, controls used, test statistics, p-values,
1922 confidence intervals, and Benjamini-Hochberg FDR corrections) for all data presented in the
1923 main and supplemental figures. Statistical information for ANOVA tests includes factors,
1924 degrees of freedom, test statistics, and post-hoc pairwise t-tests with Benjamini-Hochberg
1925 correction.

1926

1927 **S1 Video. Climbing ability of flies with knockdown of individual homologs of 3q29
1928 genes.**

1929 This video shows the climbing ability of *Elav-GAL4* control, *Cbp20* and *dlg1* individual
1930 RNAi knockdown flies at day 10 of the climbing ability experiments.

1931

1932 **S2 Video. Climbing ability of flies with pairwise knockdowns of homologs of 3q29 genes.**

1933 This video shows the climbing ability of *Cbp20/dlg1* and *Cbp20/Fsn* pairwise *Elav-GAL4*
1934 RNAi knockdown flies at day 10 of the climbing ability experiments.

1935

Table 1. Summary of major experiments for knockdown of homologs of 3q29 genes show widespread cellular and neuronal defects.

Experiment		RNAi knockdown of <i>Drosophila</i> homologs of 3q29 genes						
Phenotype	Assay	<i>Cbp20</i>	<i>dlg1</i>	<i>Cbp20/dlg1</i>	<i>Cbp20/Fsn</i>	<i>Cbp20/CG8888</i>	<i>Cbp20/Diap1</i>	<i>dlg1/Diap1</i>
Adult eye morphology	Rough eye phenotype	Rough eye	Rough eye	Enhanced rough eye	Enhanced rough eye	Enhanced rough eye	Rescue	Rescue
	Necrotic patches	None (Present in homozygous KD)	None	Yes (more severe in homozygous KD)	Yes	None	None	None
	Eye area	Decreased area	Increased area	NA	NA	NA	Rescue	Rescue
Neuronal phenotypes	Climbing ability	Climbing defects	Climbing defects	Enhanced climbing defects	Enhanced climbing defects	NA	NA	NA
	Axonal targeting	Axon targeting defects	Axon targeting defects	Enhanced targeting defects	Enhanced targeting defects	NA	Rescue	Rescue
Cell organization (pupal eye)	DLG staining	Cellular defects	Cellular defects	Enhanced cellular defects	Enhanced cellular defects	Enhanced cellular defects	Rescue	Rescue
	Phalloidin staining	Loss of photoreceptors	Loss of photoreceptors	No change	Enhanced photoreceptor loss	Enhanced photoreceptor loss	Rescue	Rescue
Cell cycle (larval eye disc)	pH3 staining	No change	No change	No change	No change	Decreased proliferation	NA	NA
	BrdU staining	No change	Increased proliferation	NA	NA	NA	NA	NA
Apoptosis (larval eye disc)	dcp1 staining	Increased apoptosis	Increased apoptosis	Increased apoptosis	Increased apoptosis	Increased apoptosis	Rescue	Rescue
	TUNEL assay	Increased apoptosis	Increased apoptosis	Increased apoptosis	Increased apoptosis	Increased apoptosis	Rescue	Rescue
Cellular phenotypes (larval wing disc)	pH3 staining	Decreased proliferation	Increased proliferation	NA	NA	NA	NA	NA
	dcp1 staining	Increased apoptosis	Increased apoptosis	NA	NA	NA	NA	NA
RNA sequencing (adult heads)	Differential gene expression	Synaptic transmission, metabolism	Synaptic transmission, ion transport	Cellular respiration, protein folding	Cell cycle, response to stimulus	NA	NA	NA

Experiment		Morpholino knockdown of <i>X. laevis</i> homologs of 3q29 genes						
Phenotype	Assay	<i>ncbp2</i>	<i>fbxo45</i>	<i>pak2</i>	<i>ncbp2/fbxo45</i>	<i>ncbp2/pak2</i>	<i>ncbp2/xiap</i>	<i>fbxo45/xiap</i>
Craniofacial morphology	Eye area	Decreased area	Decreased area	Decreased area	NA	NA	Rescue	NA
	Midbrain area	Decreased area	Decreased area	Decreased area	No change	No change	Rescue	NA
	Forebrain area	Decreased area	Decreased area	Decreased area	Decreased area	No change	Rescue	NA
Apoptosis	Cleaved caspase-3 levels	Increased caspase-3	Increased caspase-3	NA	Increased caspase-3	NA	Rescue	Rescue

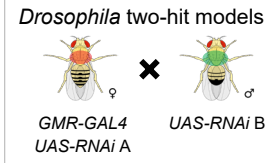
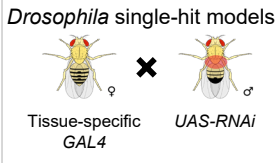
Fig. 1

Tested *Drosophila* homologs
Tested *X. laevis* homologs

	<i>ZDHC19</i>	<i>OSTalpha</i>	<i>PCYTIA</i>	<i>TCTEX1D2</i>	<i>UBXN7</i>	<i>TFRC</i>	<i>SMCO1</i>	<i>RNF168</i>	<i>WDR53</i>	<i>FBXO45</i>	<i>CG5543</i>	<i>Fsn</i>	<i>LRRK33</i>	<i>CEP19</i>	<i>PiG-X</i>	<i>Pak</i>	<i>Ulp1</i>	<i>Cbp20</i>	<i>PiG-Z</i>	<i>SENPs</i>	<i>NCBP2</i>	<i>PiG-Z</i>	<i>MFI2</i>	<i>DLG1</i>	<i>CG8886</i>	<i>BDH1</i>
<i>app</i>																										
<i>CG6836</i>																										
<i>Pcy12</i>																										

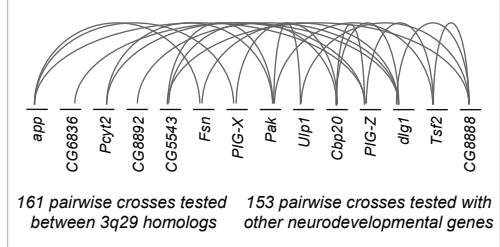
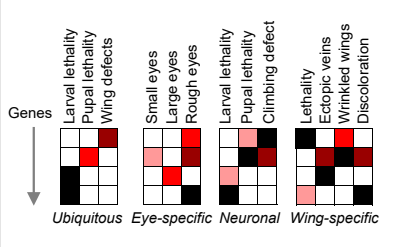
Human genes

Fly homologs



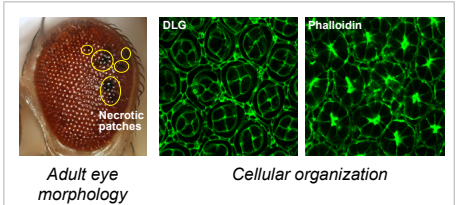
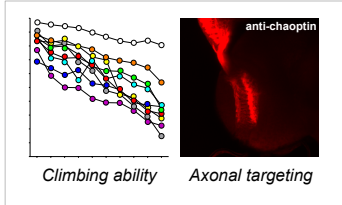
Global phenotype screening

Pairwise interaction screening

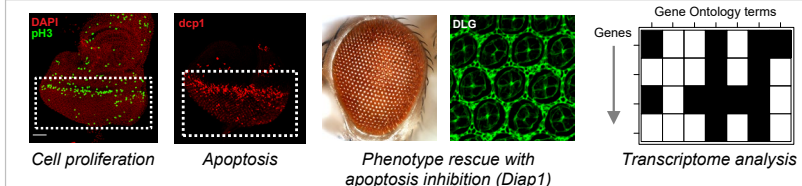


Neuronal phenotypes

Cellular phenotypes



Apoptosis and cell cycle mechanisms



Validation in *X. laevis* models

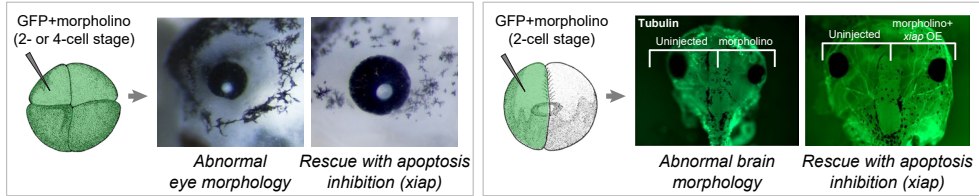


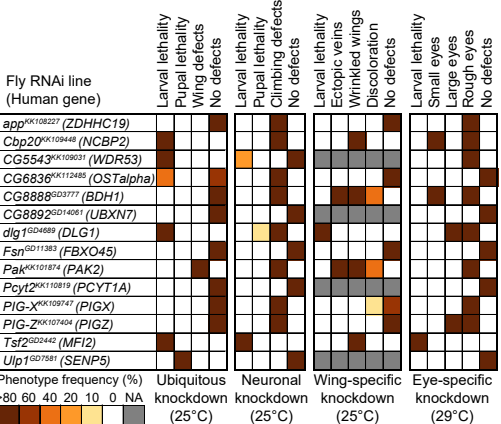
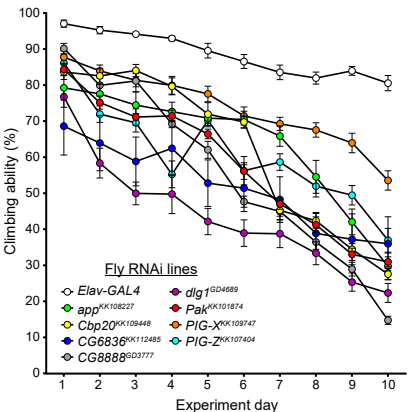
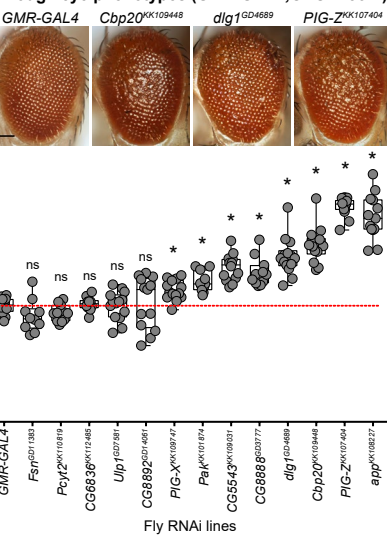
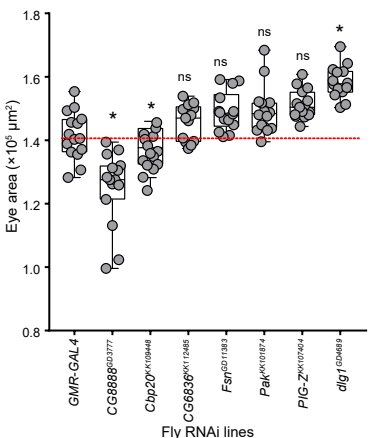
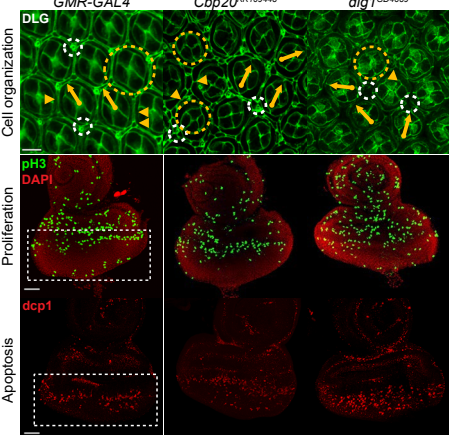
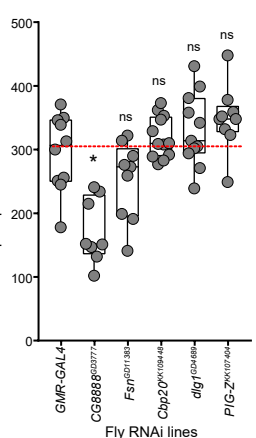
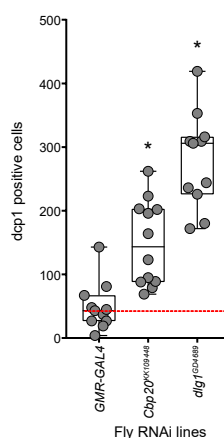
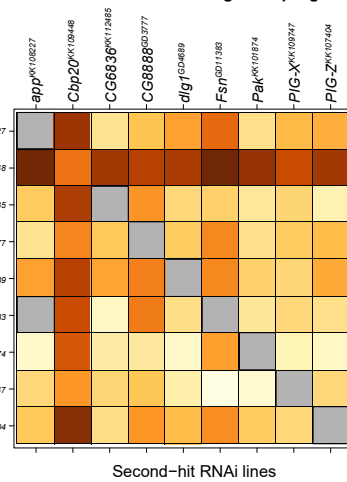
Fig. 2**A****Global phenotype screening****B****Climbing ability****C****Rough eye phenotypes (GMR-GAL4;UAS-Dicer2)****D****Adult eye area****E****Cellular phenotypes in the developing eye****F****Cell proliferation defects****G****Apoptosis defects**

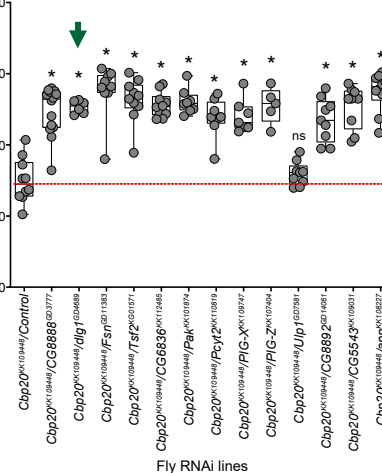
Fig. 3**A**

Pairwise interactions for homologs of 3q29 genes

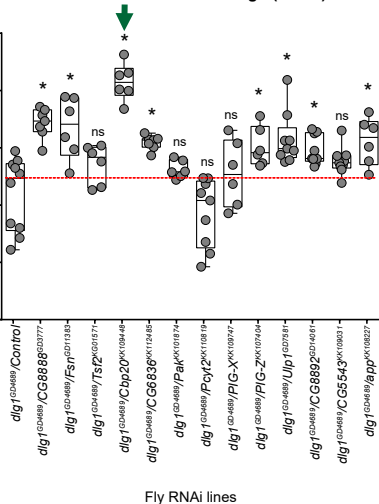
Single-hit RNAi lines



Second-hit RNAi lines

BPairwise interactions of *Cbp20* (*NCBP2*)Score change
-5 0 5 10 15 20 25 30 35 40 45 50

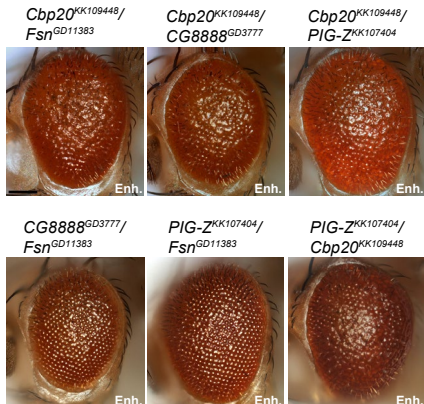
Fly RNAi lines

CPairwise interactions of *dlg1* (*DLG1*)Phenotypic score
0 10 20 30 40 50

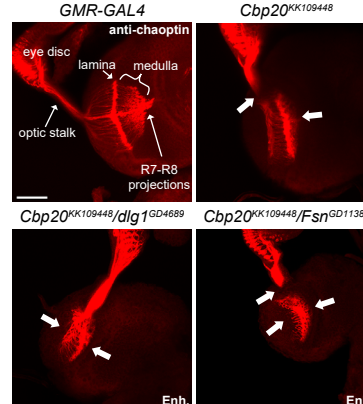
Fly RNAi lines

D

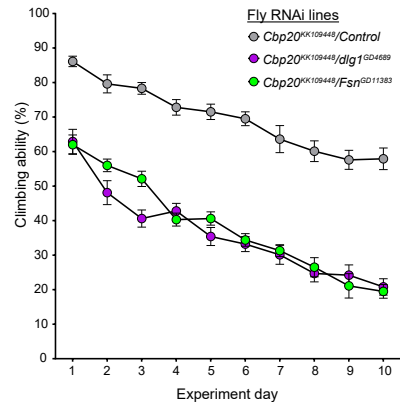
Rough eye phenotypes of pairwise interactions

**E**

Axon targeting defects

**F**

Climbing ability



Fly RNAi lines

Cbp20KK109448/Control

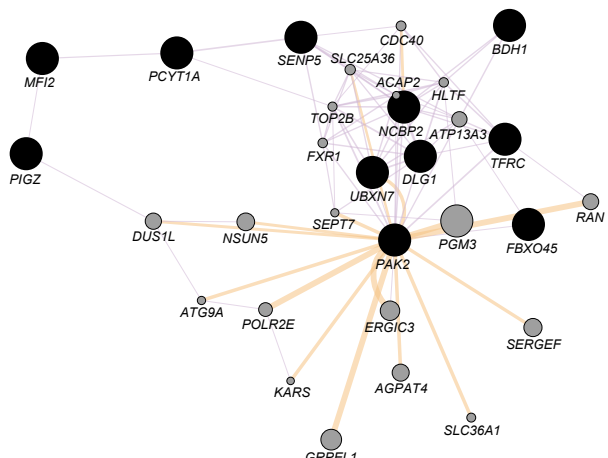
Cbp20KK109448/dlg1GD4689

Cbp20KK109448/FsnGD11383

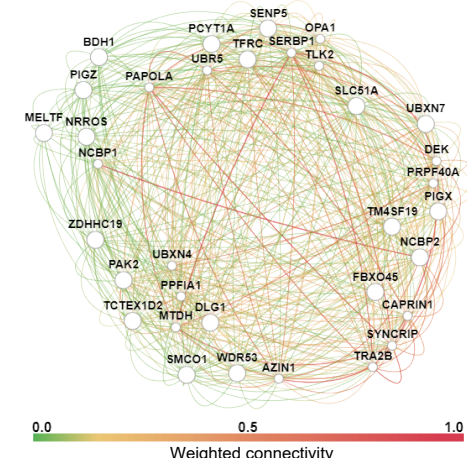
Experiment day

Fig. 4**A**

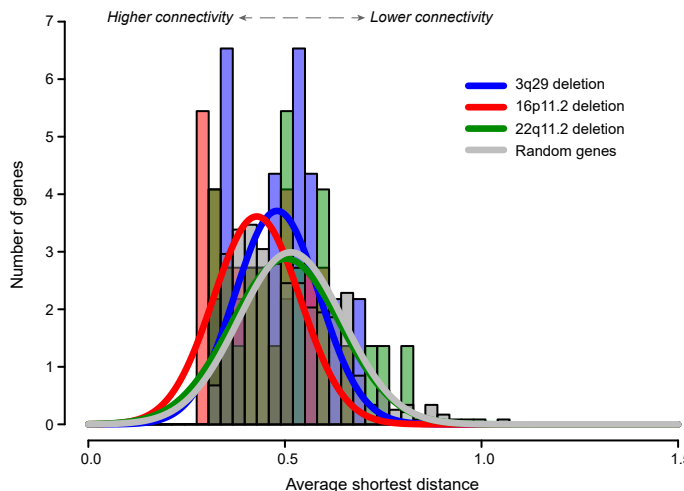
Human gene interaction network of 3q29 genes (GeneMania)

**B**

Human gene interaction network of 3q29 genes (GIANT)

**C**

Average connectivity of CNV genes in human brain-specific network

**D**

Connectivity of 3q29 genes in human brain-specific network

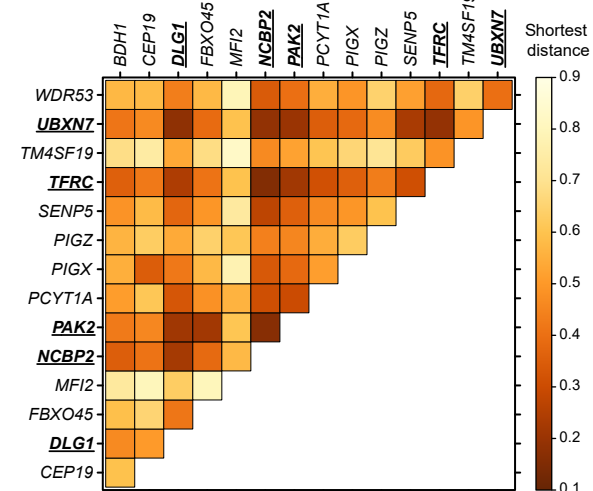
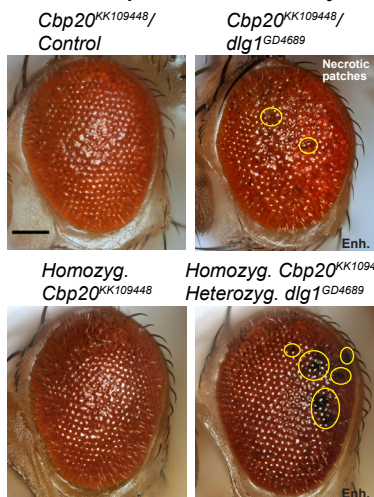
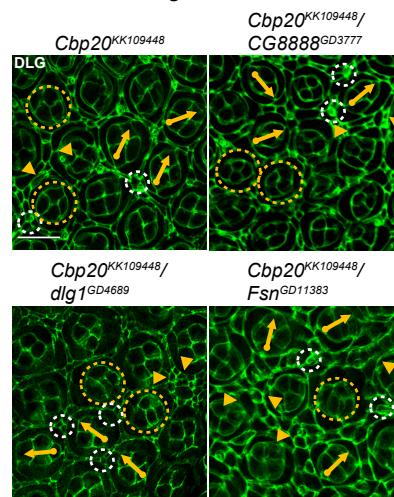
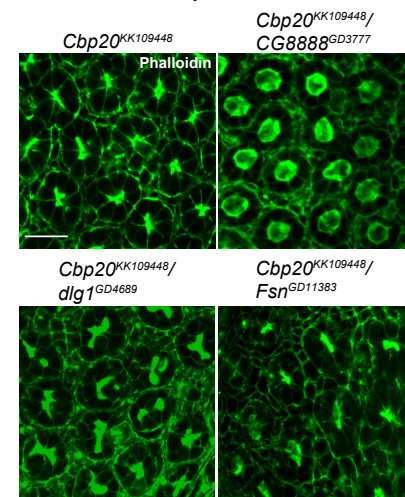
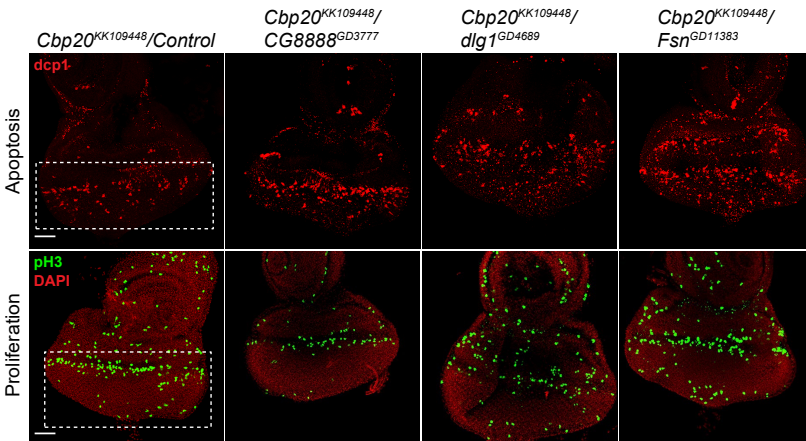
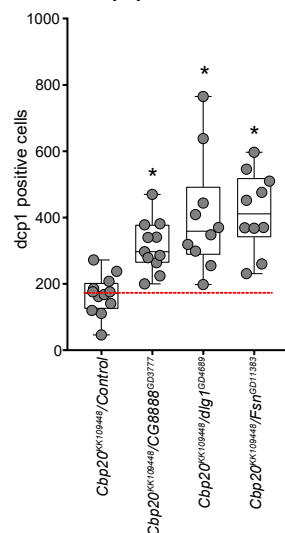
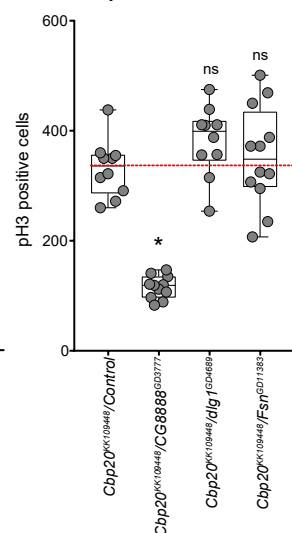


Fig. 5**A****Necrotic patches in the adult eye****B****Cellular organization defects****C****Photoreceptor cell defects****D****Cellular phenotypes of pairwise knockdowns in the larval eye disc****E****Apoptosis defects****F****Cell proliferation defects**

Fly RNAi lines

Fly RNAi lines

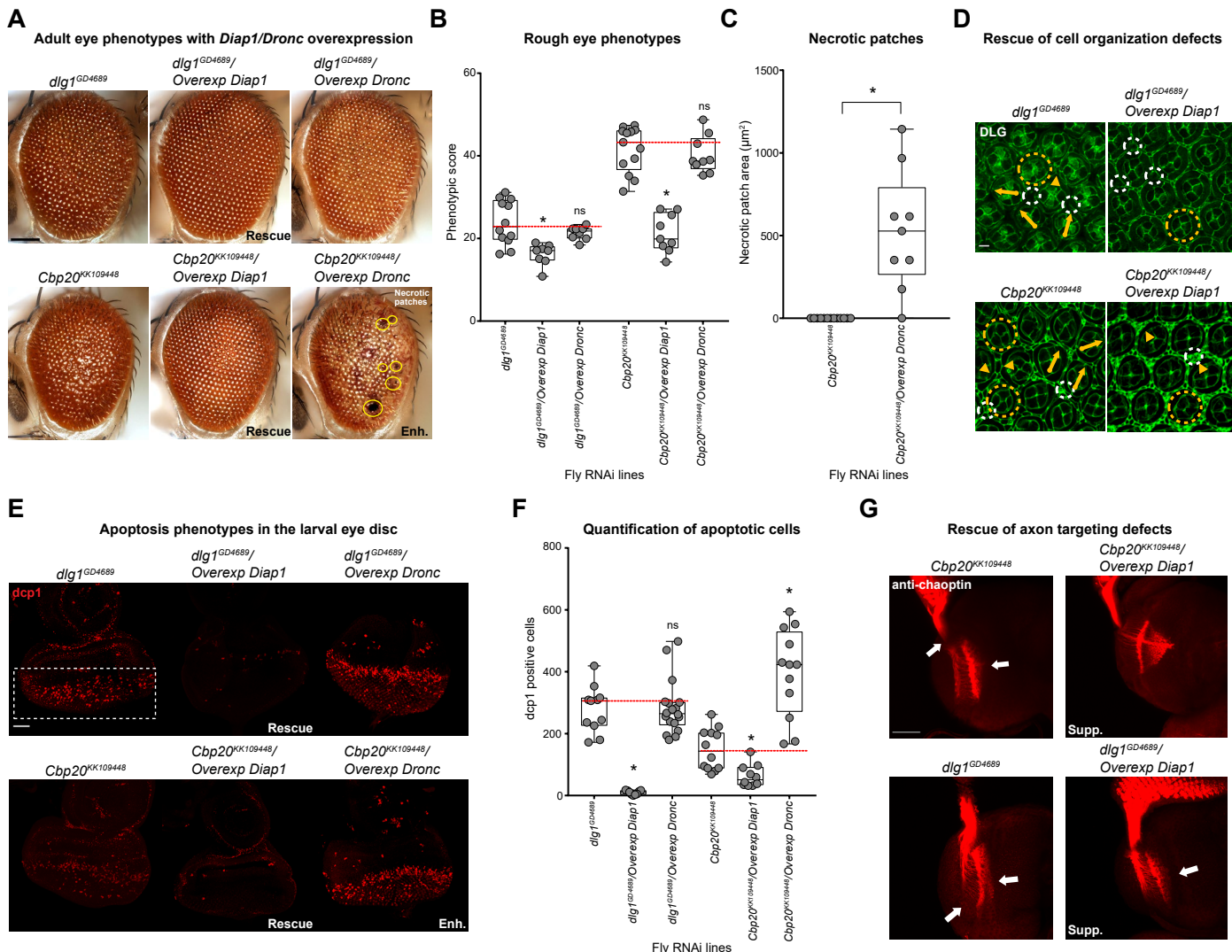
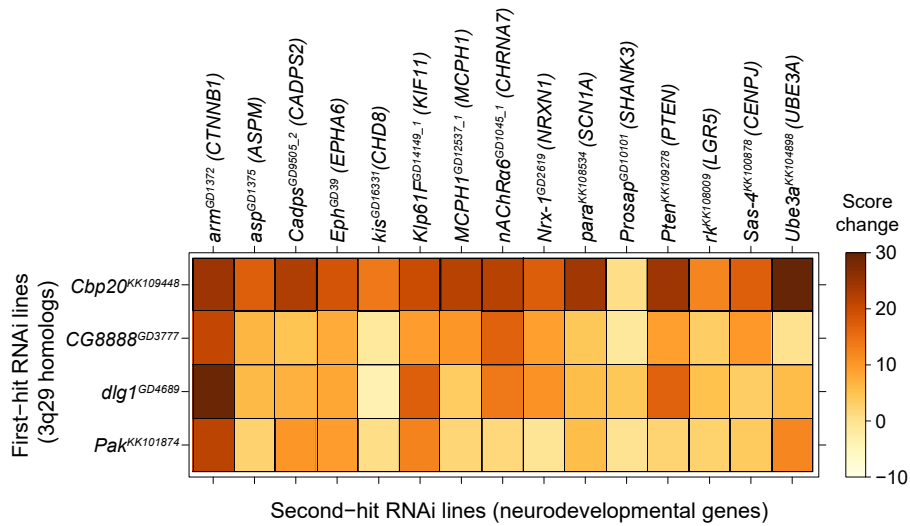
Fig. 6

Fig. 7

A

Pairwise interactions with homologs of neurodevelopmental genes

**B**

Rough eye phenotypes of pairwise interactions

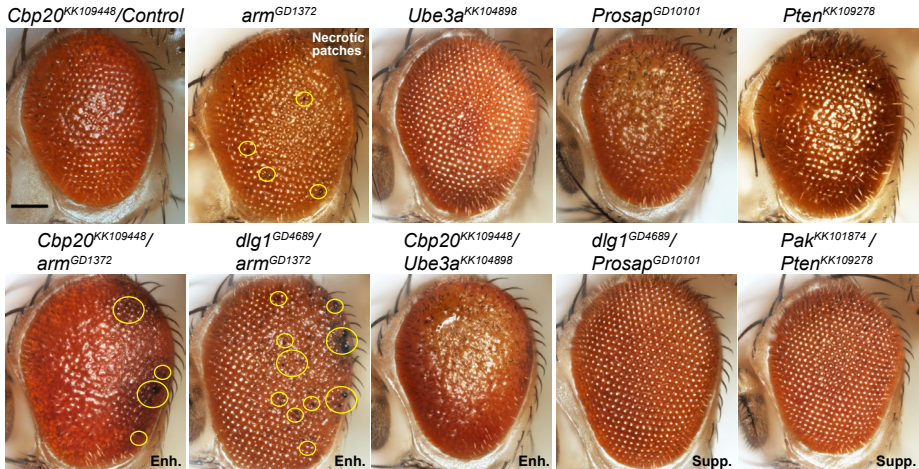


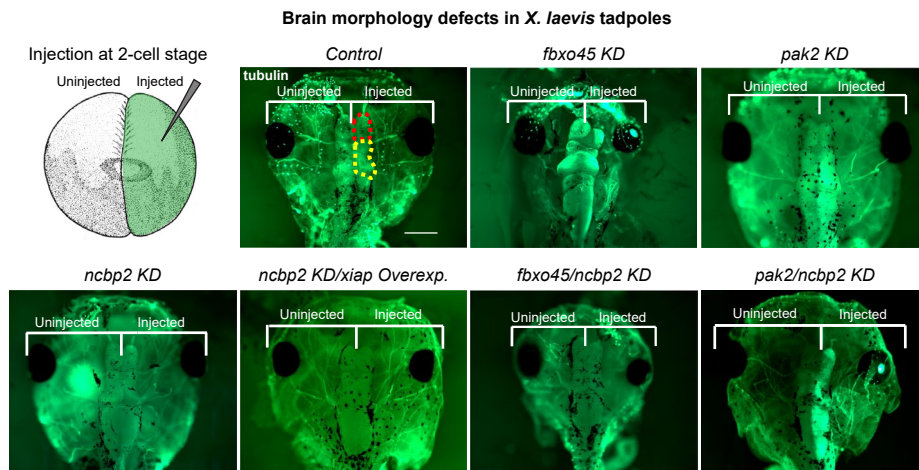
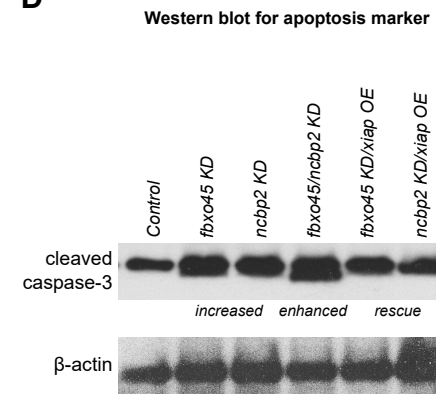
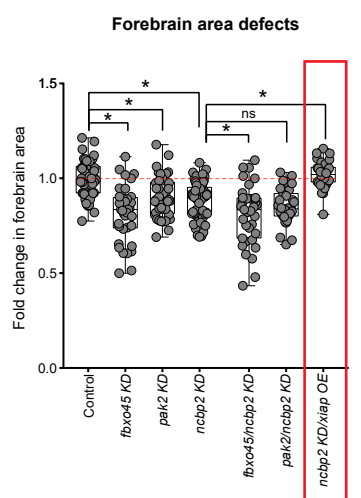
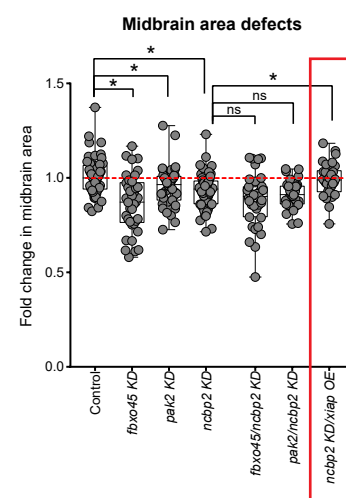
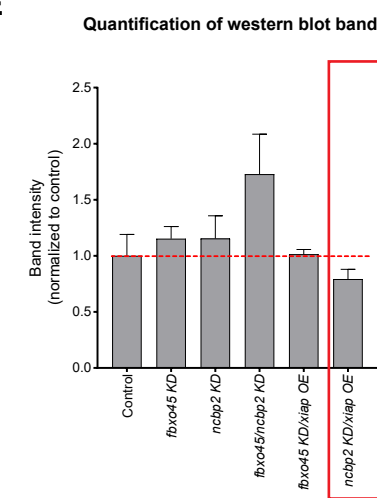
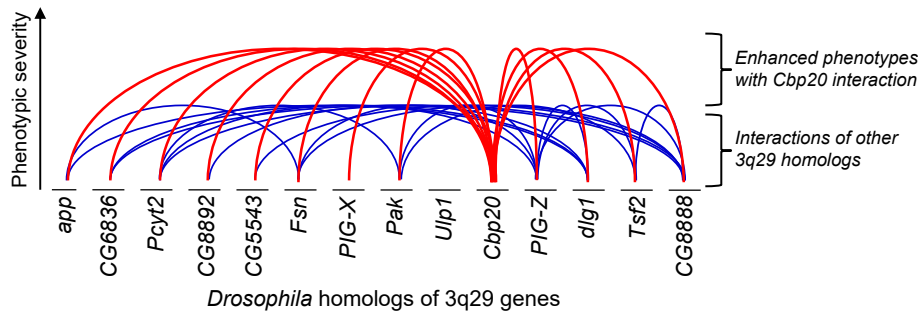
Fig. 8**A****D****B****C****E**

Fig. 9

A



B

